Mandibular Reconstruction Using Bioactive 3D-Printed Porous Polyetherketone Scaffolds and Mesenchymal Stem Cells

Michael Roskies, BSc, MD, FRCSC
Department of Otolaryngology – Head & Neck Surgery, McGill University
November 2017

A thesis submitted to McGill University in partial fulfillment of the requirements of the degree of Master of Science in Otolaryngology – Head and Neck Surgery

Abstract

Objective: Additive manufacturing (or 3D Printing, 3DP) offers a tailored approach to tissue engineering by providing anatomically precise, scaffolds onto which stem cells and growth factors can be supplied. Polyetherketoneketone (PEKK), an ideal candidate biomaterial, is limited by a poor implant-bone interface, but can be functionalized with adipose-derived stem cells (ADSC) to promote integration. This study examined the interaction of mesenchymal stem cells with 3DP polyetherketone scaffolds. A subsequent in vivo study was done studying the 3DP PEKK/ADSC composite within the critical-sized mandibular defect of a rabbit model.

Study Design/Methods: After characterization of stem cells using alamar blue, alkaline phosphatase and scanning electron microscopy, twelve trapezoidal porous scaffolds with dimensions of 1.5 x 1.0 x 0.5 cm were printed using selective laser sintering (SLS). ADSCs were seeded on the scaffolds that were then implanted in marginal defects created in New Zealand rabbits. Rabbits were euthanized at 10- and 20-week intervals. Microcomputed tomography (microCT) was used to characterize bone ingrowth and was correlated with histological analysis. Stress testing was performed on the scaffolds before and after implantation.

Results: PEEK scaffolds maintained the viability of both ADSCs and bone marrow-derived stem cells (BMSCs); however, ADSCs demonstrated higher osteodifferentiation than BMSCs. All scaffolds with ADSCs were well integrated into adjacent bone. Bone-to-tissue volume increased from 30.34% (+/-12.46) to 61.27% (+/-8.24) and trabecular thickness increased from 0.178 mm (+/-0.069) to 0.331 mm (+/-0.0306) in the 10 and 20-week groups, respectively compared to no bone regrowth on the control side ($p<0.05$). Histology confirmed integration at the bone-implant interface. Biomechanical testing revealed a compressive resistance fifteen times that of bone alone ($p <0.05$)

Conclusion: 3D-printed PEKK scaffolds combined with ADSCs present a promising solution to improve the bone-implant interface and increase the resistance to forces of mastication after mandibular reconstruction.

Resumé

Objectif: L'impression 3D (I3D) offre une approche unique à la reconstruction des défauts cervicofacials en fournissant des échafaudages anatomiquement précis sur lesquels des cellules souches et des facteurs de croissance peuvent être cultivé. Le polyetherketoneketone (PEKK), un candidate idéal, est limitée par leur mauvaise intégration avec l'os adjacent, mais peut être « fonctionnalisée » avec des cellules souches dérivées d'adipose (ADSC) pour favoriser l'intégration. Cette étude a examiné l'interaction des cellules souches mésenchymateuses avec les échafaudages 3DP polyetherketone. Une étude in vivo ultérieure a été effectuée en étudiant le composite 3DP PEKK / ADSC dans le défaut mandibulaire de taille critique d'un modèle de lapin.
Méthode: Après la caractérisation des cellules souches utilisant du « alamar blue », « alkaline phosphatase » et « scanning electron microscopy », on a imprimé douze échafaudages poreux trapézoïdaux avec des dimensions de 1,5 x 1,0 x 0,5 cm en utilisant « selective laser sintering » (SLS). Les ADSC ont été isolées de lapins et cultivées sur ces échafauds. Des défauts de taille critique ont été créés de chaque côté ; les échafauds ont été implantés sur la droite, la gauche servant de contrôle. À des intervalles de 10 et 20 semaines, un microCT, une analyse histologique et des tests de résistance ont été faits pour caractériser la croissance osseuse.
Résultats: Les échafaudages PEEK ont maintenu la viabilité des ADSC et des BMSC; Cependant, les ADSC ont démontré une ostéodifférenciation plus élevée que les BMSC. Tous les échafaudages avec ADSC ont bien intégrés dans l'os adjacent. Le volume des tissus osseux a

augmenté de 30,34% (+/- 12,46) à 61,27% (+/- 8,24) et l'épaisseur trabéculaire a augmenté de 0,178 mm (+/- 0,069) à 0,331 mm (+/- 0,0306) dans le 10- et les groupes de 20-semaines, respectivement par rapport à la non-croissance osseuse du côté controle ($p < 0,05$). L'histologie a confirmé l'intégration à l'interface os-implant. Les tests biomécaniques ont révélé une résistance à la compression quinze fois celle de l'os seul ($p < 0,05$).

Conclusion : Les échafauds PEKK imprimés par la fabrication additive en combinaison avec des ADSC offrent une solution viable pour faciliter l'intégration de l'os-implant en attendant une reconstruction osseuse cervico-faciale.

Table of Contents

Preface

Contributions of authors

Michael Roskies was responsible for the literature review in its entirety, the experimental design, data collection, analysis of results and drafting of both manuscripts. Simon Tran, Dongdong Fang, Mohamed Nur-Abdallah and Jack Jordan assisted in the conception and data collection for the first manuscript. Simon Tran, Dongdong Fang, Mohamed Nur-Abdallah and André Charbonneau assisted in the conception and data collection for the second manuscript. Dr. Michael Hier provided expertise on the surgical procedures performed. Simon Tran, Faleh Tamimi, Dongdong Fang, Mohamed Nur-Abdallah, Mohamed Bakkar, Li Chieh-Lin and André Charbonneau assisted in the conception and data collection for the book chapter.

Claim of originality

The original idea for the creation of 3D printed polyetherketone scaffolds with stem cells for mandibular reconstruction was the work of Michael Roskies. No prior study has examined the combination of 3D printed thermoplastic with adipose stem cells for mandibular reconstruction in an animal model.

Acknowledgments

Research funding was provided by the Natural Sciences and Engineering Research Council of Canada (NSERC), Canadian Institutes of Health Research (CIHR), Fonds de Reserche du Québec – Santé (FRSQ) and the McGill Department of Otolaryngology – Head and Neck Surgery. Thank you to Dr. Saul Frenkiel for his support from the onset of this project. This work could not have been done without the mentorship of my supervisors Dr. Simon Tran and Dr. Michael Hier. I am indebted to Dr. Hier for his mentorship, support and guidance throughout my career. The work done at the Canadian Craniofacial Stem Cell and Tissue Engineering Laboratory at McGill University is of the highest quality in this academic sphere; it's members, Dongdong Fang, Jack Jordan, Mohamed Nur Abdallah and André Charbonneau, have propelled this work to levels it could not have achieved otherwise. Finally, thank you to my supportive family and especially my wife Marissa, without whom, none of this would be worth it.

1 Introduction

1.1 Objectives and hypothesis

This manuscript-based Master's thesis includes two studies, one in vitro and another in vivo. Both were conducted in sequence to determine the optimal composition of a tissue engineered implant for mandibular reconstruction using polyetherketone (PEK) and mesenchymal stem cells. A book chapter was written further describing our laboratory's approach to this in vivo project. PEK is a bioinert thermoplastic that has been investigated for its potential use in craniofacial reconstruction, however, its use in clinical practice is limited by a poor integration with adjacent bone upon implantation. The initial phase compared the biocompatibility of two sources of stem cells (bone-marrow and adipose derived) with a 3D printed polyetheretherketone (PEEK) scaffold. The follow up used the ideal combination of adipose-derived stem cells and polyetherketoneketone (PEEK) in an animal model to determine adjacent bone integration and changes in biomechanical properties.

2 Review of Relevant Literature

2.1 Application of 3D printing for biomaterials research

Additive manufacturing has many applications in the printing of biomaterials. The main advantage of 3D printing is the ability to print on demand three-dimensional complex structures that are accurately reproducible, but also highly customizable (which makes it an ideal application in medicine). 3D printing has been used in otolaryngology for tissue engineering of auricles for pediatric microtia (1), as a bioresorbable airway splint created with a three-dimensional printer (2) and in simulation for temporal bone surgery.(3) Cohen et. al used 3D printing (3DP) to model mandibles for pre-operative plating. They state that 3DP is a precise, fast, and cheap approach to

mandibular reconstruction.(4) The benefits can be seen for patients (shortened operation time), surgeons (improved cosmesis) and healthcare systems (cost savings) alike

2.2 Mesenchymal stem cells increase osseointegration of scaffolds

Mesenchymal stem cells (MSCs) are needed for osseoinegration. Garcia-Gareta et. al showed how bone tissue engineering effectively combines cells and scaffolds in vitro to replace damaged or lost bone in vivo. This study showed that in bony defects of mature mule sheep femoral condyles that had a large gap, seeding MSCs resulted in a higher implant-bone contact are and implant-bone fixation strength.(5) Other studies have shown the combination of porous scaffolds with MSCs can repair osteochondral defects. Jeong et al. used a scaffold made of MSCs and polydioxanone/polyvinyl alcohol hybrid scaffold for femoral head reconstruction in rabbits. They showed that the physical stability of the implant was maintained at 4 weeks and expression of cartilage-specific genes was seen. The hybrid started to resemble that of cartilage in vivo and strongly stained for type II collagen.(6) Zamiri et al. successfully loaded human cadaveric allogenic bone scaffolds with patient-autologous MSCs to reconstruct mandibular defects in 2 of 3 patients. (7)

2.3 Polyetherketones in other medical fields

As a scaffold, polyetherketons represent an ideal candidate and is commonly employed in other fields as a biomaterial. Steinberg et al. used carbon-reinforced PEEK (CF-PEEK) implants in orthopedic surgery.(8) Mobbs et al. used biphasic calcium phosphate ceramic contained within a PEEK cage as an effective implant for use in anterior cervical spine surgery.(9)

2.4 Polyetherketones in craniofacial reconstruction

PEK's use in craniofacial reconstruction is limited to case reports and none describe mandibular reconstruction as its ability to withstand load-bearing forces has not been established.

Kim et al. showed that customized PEEK could be used in 4 patients with midface defects and that each had had excellent postoperative aesthetic and functional results.(10) No study to date has examined PEK (either PEEK or PEKK) for load-bearing craniofacial reconstruction.

2.5 Thesis rationale

In view of the above stated need for bioactive, tissue-engineered, load-bearing mandibular implants for reconstruction, this thesis set out to examine the relationship of bioinert, biomechanically resistant PEK scaffolds and bioactive mesenchymal stem cells for this purpose.

3 Manuscript 1

***Roskies M**, Jordan J, Fang D, Nur-Abdallah M, Tamimi F, Tran S. (2016) Improving PEEK bioactivity for craniofacial reconstruction using a 3D printed scaffold embedded with mesenchymal stem cells. J Biomater Appl. 31(1): 132-139.*

3.1 Abstract

Objective: Polyetheretherketone (PEEK) is a bioinert thermoplastic that has been investigated for its potential use in craniofacial reconstruction, however, its use in clinical practice is limited by a poor integration with adjacent bone upon implantation. To improve the bone-implant interface, two strategies have been employed: to modify its surface or to impregnate PEEK with bioactive materials. This study attempts to combine and improve upon the two approaches by modifying the internal structure into a trabecular network and to impregnate PEEK with mesenchymal stem cells. Furthermore, we compare the newly designed PEEK scaffolds' interactions with both bone-derived (BMSC) and adipose (ADSC) stem cells.

Design: Customized PEEK scaffolds were designed to incorporate a trabecular microstructure using a computer-aided design program and then printed via selective laser sintering (SLS), a 3D-printing process with exceptional accuracy. The scaffold structure was evaluated using microCT. Scanning electron microscopy (SEM) was used to evaluate scaffold morphology with and without mesenchymal stem cells (MSCs). Adipose and bone marrow mesenchymal cells were isolated from rats and cultured on scaffolds. Cell proliferation and differentiation were assessed using alamarBlue and alkaline phosphatase assays, respectively. Cell morphology after 1 week of co-culturing cells with PEEK scaffolds was evaluated using SEM.

Results: SLS 3D printing fabricated scaffolds with a porosity of 36.38% ± 6.66 and density of 1.309 g/cm^2. Cell morphology resembled viable fibroblasts attaching to the surface and micropores

of the scaffold. PEEK scaffolds maintained the viability of both ADSCs and BMSCs; however, ADSCs demonstrated higher osteodifferentiation than BMSCs ($p < 0.05$).

Conclusions: This study demonstrates for the first time that SLS 3D printing can be used to fabricate customized porous PEEK scaffolds that maintain the viability of adipose and bone marrow derived MSCs and induces the osteodifferentiation of the adipose derived MSCs. The combination of 3D printed PEEK scaffolds with MSCs could overcome some of the limitations using PEEK biopolymers for load-bearing bone regeneration in craniofacial reconstruction.

3.2 Introduction

Current therapies for bone regeneration involve biomaterials like natural polymers, ceramics and titanium that are limited by weak mechanical properties, extended degradation time, low compressive strength and potential metal ion release (11-13). As such, synthetic polymers like polyetheretherketone (PEEK) are gaining popularity in the fields of orthopedics, neurosurgery and trauma (14-17). Polyetheretherketone (PEEK) is a thermoplastic biomaterial organized in a linear homopolymer composed of 100 monomer units. This chemical structure confers stability at high temperatures (exceeding 300°C) allowing it to be sterilized repeatedly and offering resistance to radiation damage without experiencing any degradation in mechanical properties or biocompatibility (18). In comparison to conventional implants like titanium, PEEK exhibits an elastic modulus comparable to that of cortical bone to reduce the occurrence of stress shielding (19). Also, PEEK is radiolucent thus mitigating interference and artifacts in x-rays and MRIs during cancer surveillance surrounding reconstructed defects (20).

Not surprisingly, PEEK's use in craniofacial reconstruction is well-described (10); however, it's use in load-bearing applications is limited due to a lacked capacity for direct bone apposition and consequent bony fixation (15, 21). To increase fixation to surrounding bone, the techniques studied have included post-fabrication surface modification of the construct or impregnating the scaffold with bioactive materials (14, 22). These strategies, however effective, prove to be time consuming, require a special skillset and are imprecise.

Advances in rapid prototyping (known commonly as 3D printing) have introduced the ability to fabricate customized scaffolds with complex internal geometries. Selective laser sintering (SLS), a form of rapid prototyping, selectively heats two dimensional slices of a particular substrate with a CO_2 laser and then sinters the slices together along the y-axis, creating the desired three-dimensional shape (23). SLS has the advantages of offering good control over microstructure design, allowing the user to incorporate a trabecular network into PEEK scaffolds that closely mimic the shape of bone. Additionally, SLS can be combined with tissue engineering concepts to provide an interconnected network through which progenitor cells can migrate (24, 25). While the use of manually-produced PEEK blocks and osteoprogenitor cells has been evaluated in vitro (26), the combination of an SLS-printed scaffold with stem cells has yet to be evaluated. Mesenchymal stem cells (MSC) are self-renewing and multipotent, making them ideal for regenerative medicine (27). When combined with biomaterials, MSCs derived from either bone marrow (BMSC) or adipose tissue (ADSC) can differentiate into osteoblasts, resulting in increased osteointegration (28-30); however the ideal combination of MSCs and biomaterial scaffolds for bone regeneration is still unclear.

The aim of this study is to evaluate the interaction of a customized selective laser sintered PEEK scaffold with rat BMSCs versus rat ADSCs. Specifically, we aim to characterize BMSC and ADSC

proliferation, differentiation and integration into the scaffolds in vitro in the hopes of providing the basis for alternative therapies of load-bearing craniofacial bony defect regeneration.

3.3 Materials and Methods

3.3.1 Design, printing and characterization of scaffolds

Design of the scaffolds was done using a computer-aided design software (Autodesk Within Medical, version 4, CA, USA). Ten identical 5 cm x 1 cm x 1 cm rectangular structures were generated with repeated trabecular subunits embedded within them (**Figure 3.1, A-E**).

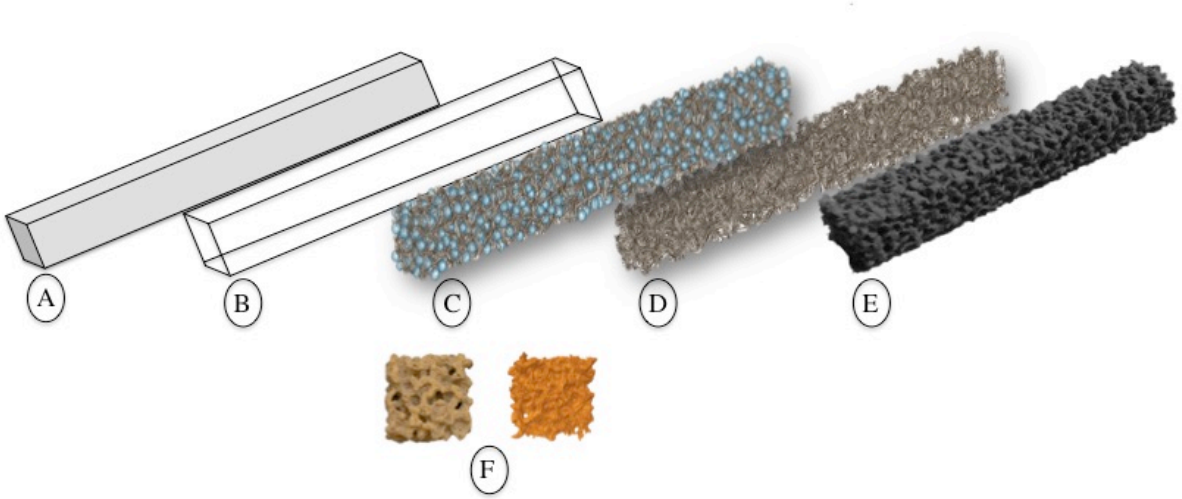

Figure 3.1 Computer aided design of the porous PEEK scaffolds. (a) Creation of a rectangular bounding box, (b) the rectangular beam hollowed out, (c) trabecular structures embedded with pores identified (blue), (d) final lattice, (e) final construct. (f) Final printed construct, (g) MicroCT image of the printed scaffold

The 3D structure was then manufactured using the EOSINT P800 SLS printer (Solid Concepts, Valencia, CA, USA). Briefly, the SLS technique employs a CO_2 laser to sinter thin layers of PEEK powder together at its melting point in a successive two-dimensional fashion along the x-axis in order to build a 3D solid form construct along the y-axis. The EOSINT P800 offers a resolution density of 1.30 g/cm^3, a layer thickness of 120µm at building speeds of up to 10mm/hour (31).

Once complete, the final rectangles were cut into 1.0 cm^3 cubes suitable for placement into 24-well cell culture plates (**Figure 3.1, F**). A high-pressure steam sterilizer (Yamato SM 300, Yamato Scientific, Japan) was used to autoclave the cubes at 121°F for 12 minutes.

Microcomputed tomography (microCT) scans were performed using a SkyScan 1172 instrument (Bruker-Microct, Kontich, Belgium) and analysis software (Version 2.2f, Skyscan, Kontich, Belgium). The x-ray source was operated at 60 kV/167 μA with a 0.5-mm Al filter. Images were acquired with a rotational step of 0.4 degrees. Porosity (total porosity, open porosity and closed porosity) and pore size were evaluated using CTAn software (Version 1.13.11, Skyscan, Kontich, Belgium). PEEK density was determined using helium pycnometry (Accupyc 1330, Micromeretics, Bedfordshire, UK).

3.3.2 Isolation and expansion of rat MSCs

Bone marrow and adipose derived stem cells were isolated from 5-7 week old Sprague-Dawley rats. The collection and isolation of the stem cells were carried out in accordance with established protocols described by Maniatopolous and Bunnell et al. (32, 33). After isolation, the adherent cells were cultivated in an Alpha Minimum Essential Medium (α-MEM) culture medium (Gibco BRL, Grand Island, NY, USA,) supplemented with 15% bovine fetal serum and 1% penicillin/streptomycin at of 37°C and 5% CO_2 for a period of 7 days. Media was changed every 3-4 days until colonies of fibroblast-like cells were observed. Before reaching confluence of 70-80%, the cultured cells were washed with 0.25% trypsin EDTA (Gibco, USA) before resuspension in culture media for re-expansion. Third passage (P3) cells were used for this experiment.

3.3.3 Characterization of rat BMSC and ADSC

The adipogenic, chondrogenic and osteogenic phenotypes of the ADSCs and BMSCs were examined as a proof of cell multipotency. Adipogenesis was done using protocols laid out by Bruedigam (34) and characterized with Oil Red O (Sigma Aldrich, MO, USA) staining. Chondrogenesis was done using the "Mesenchymal Stem Cell Identification Kit" (R&D Systems, MN, USA) and characterized with immunofluorescence staining for collagen type II. Osteogenesis was done using protocols laid out by Eijken (35) and characterized using Alizarin Red (Sigma-Aldrich, MO, USA) staining. Cellular imaging and analysis was done using Volocity 3D Image Analysis Software™ (version 4.5.1).

3.3.4 Submersion of scaffolds in cell growth medium

In order to increase the amount of bone formation into the porous scaffold, a negative pressure syringe method was used (36). After sterilization, the scaffolds were transferred into 60 ml syringes filled with 20 ml normal cell growth media. At a negative pressure of 100 kPa, vibration was applied to the syringe to release effervescence for 100 seconds. The scaffolds were then submerged in medium of 24 well plates to avoid aeration. Cells were then seeded at a density of 4200 cells/cm^2.

3.3.5 Proliferation and differentiation assays

AlamarBlue assay (Invitrogen, NY, USA) was used to measure cell viability (a measure of cell proliferation). The assay displays a fluorometric/colorimetric growth indicator as a result of oxidation-reduction metabolic activity. With cellular proliferation, the resulting fluorescence was read at 100µl increments using a spectrophotometer (Spectramax M2E, Molecular Devices, CA, USA) and the results were plotted (as a percentage relative to the positive control).

For osteogenic differentiation, alkaline phosphatase assay (ALP), a biomarker of bone mineralization, was used. After cell seeding on the PEEK scaffolds in a 24-well plate, the "experimental group" was immersed in osteogenic differentiation media comprised of α-MEM, dexamethasone, β-glycerophosphate, 2-mercaptoethanol and ascorbic acid. Every 2-3 days for the period of 28 days, the media was replaced and the cells were examined. After sonication, p-nitrophenyl phosphate tablets were added to the supernatant which was then incubated for 1 hour. A plate reader (Bio-Tek Instruments, state, country) was used to quantify the results. BMSC and ADSC cells immersed in osteogenic differentiation media, but without the scaffold, served as "positive controls" for osteogenic differentiation. BMSC and ADSC seeded on the scaffold, but immersed in basal growth media, (i.e. with no osteogenic differentiation additives) served as "negative controls".

3.3.6 Scanning electron microscopy

For visualizing cell morphology on the PEEK scaffolds, samples were washed with phosphate-buffered saline (PBS) and then fixed in 2.5% glutaraldehyde for at least 24 h at 4 ^{o}C. Afterwards, the samples were rinsed with PBS and dehydrated by incubating consecutively in 30%, 50%, 70%, 90% ethanol and then two times in 100% ethanol for 10 min. Samples were dried with hexamethyldisilazane (HMDS) and then finally sputter-coated with platinum. Samples were analyzed using a scanning electron microscope (SEM) (FEI Inspect F-50 FE-SEM, FEI Inc, Hillsboro, Oregon, USA).

3.3.7 Statistical Analysis

Intergroup differences between experimental and control groups at different time points were compared using t-tests (SPSS 11.0). Differences were considered significant at *P* values <0.05.

3.4 Results

Scaffolds were 10 x 10 x 10 mm in size. Micro-CT analysis showed that PEEK scaffolds had a total porosity of 36.38 ± 6.66, an open porosity of 35.08 ± 6.40, and a closed porosity of 2.05 ± 0.67. Density of the scaffolds after being autoclaved was preserved and was determined by pycnometry to be 1.309 g/cm^2 + 0.001 (N = 6) (**Figure 3.1, G**).

As a proof of multipotency, multi-lineage differentiation was examined on both the BMSC and ADSC used in this in vitro study. This is to ensure the cells used maintained the ability to renew as unspecialized cells, but still retain the ability to specialize, otherwise known as

'stemness'. **Figure 3.2** depicts the several cell differentiation assays carried out.

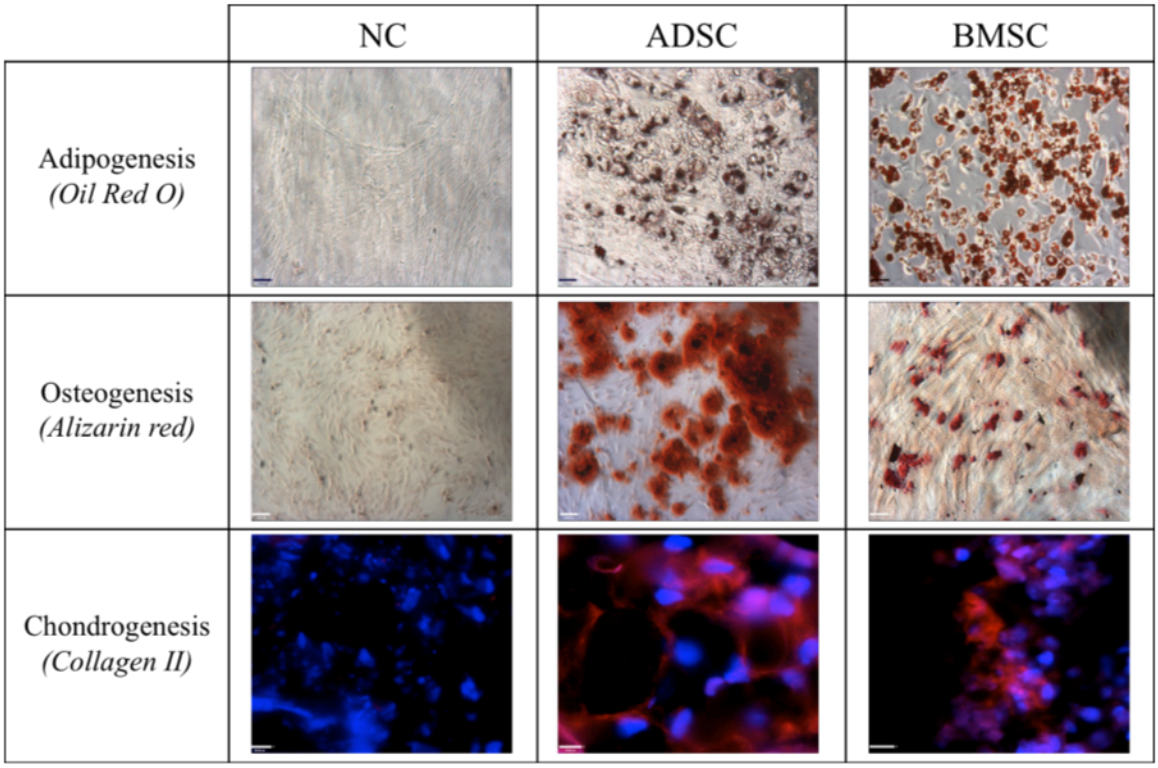

Figure 3.2 Multilineage differentiation of adipose-derived stem cells (ADSC) and bone marrow derived stem cells (BMSC) versus the negative control (NC). Scale bars for oil red and alizarin red (66 μm) and collagen II (20 μm)

After 3 weeks of induction, osteogenic differentiation was visualized with Alizarin red staining: both ADSC and BMSC differentiated into osteocytes as depicted by calcium mineralisation, whereas the normal control (acellular media) did not. After 28 days, adipogenic differentiation was visualized with Oil Red O staining: both ADSC and BMSC differentiated into adipocytes as depicted by the presence of neutral lipids and cholesteryl esters, but not biological membranes, whereas the normal control did not. Immunofluorescence microscopy of collagen type II was observed in ADSC and BMSC after 28 days, indicating chondrogenic differentiation. This was not observed in the normal control. Both cell groups were able to differentiate into all 3 cell types demonstrating their multipotency.

Cell viability and proliferation of cells on the PEEK scaffold was measured at days 1, 3 and 5 (**Figure 3.3**)

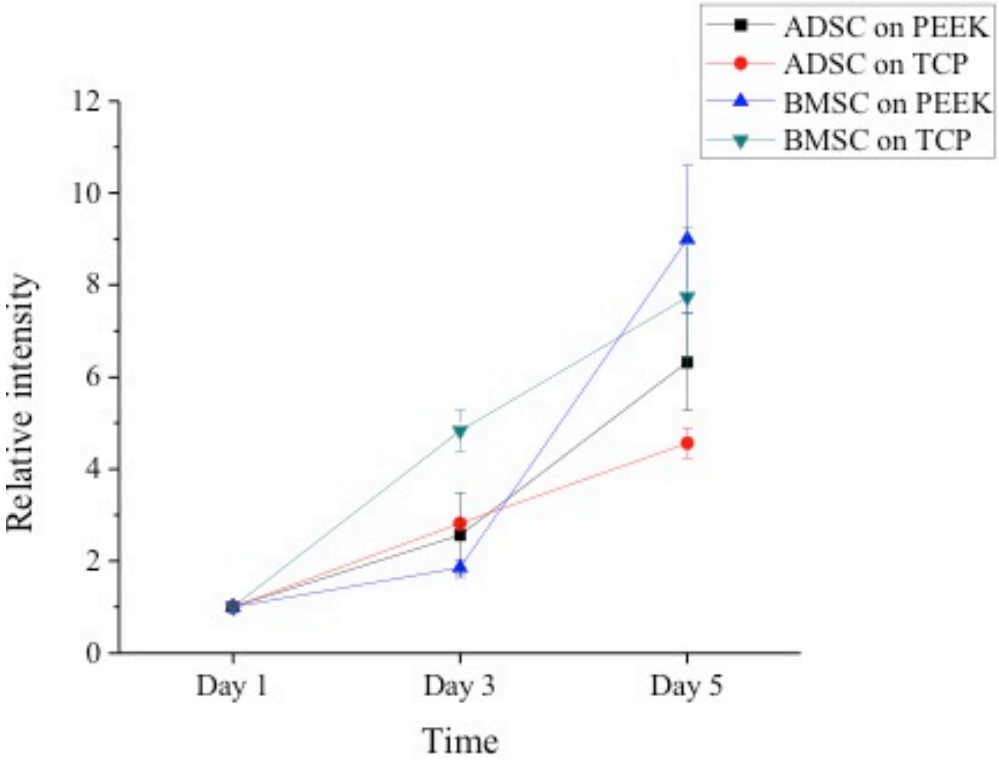

Figure 3.3 Alamar blue assay at days 1, 3 and 5 of ADSC and BMSC plated in osteogenic growth media alone on a tissue culture plate (TCP) versus with PEEK scaffold. Relative intensity is a standardized measure of growth rates versus the first day of cell seeding (N=8).

As cell count increases in the growth medium, so too does the fluorescence in the 24-well plate as demonstrated by the alamarBlue assay. BMSC and ADSC showed higher proliferation rates on scaffold (compared to positive controls).

Cell differentiation was quantified at day 28 after cell lysis to measure alkaline phosphatase (ALP) activity. **Figure 3.4** shows that the PEEK scaffold group with ADSCs and osteodifferentiation media displayed similar ALP activity to the positive control (ADSCs with osteodifferentiation media) and much greater ALP activity to the negative control (scaffold,

ADSCs and growth media). However, that scaffolds embedded with BMSCs show higher variability in ALP activity.

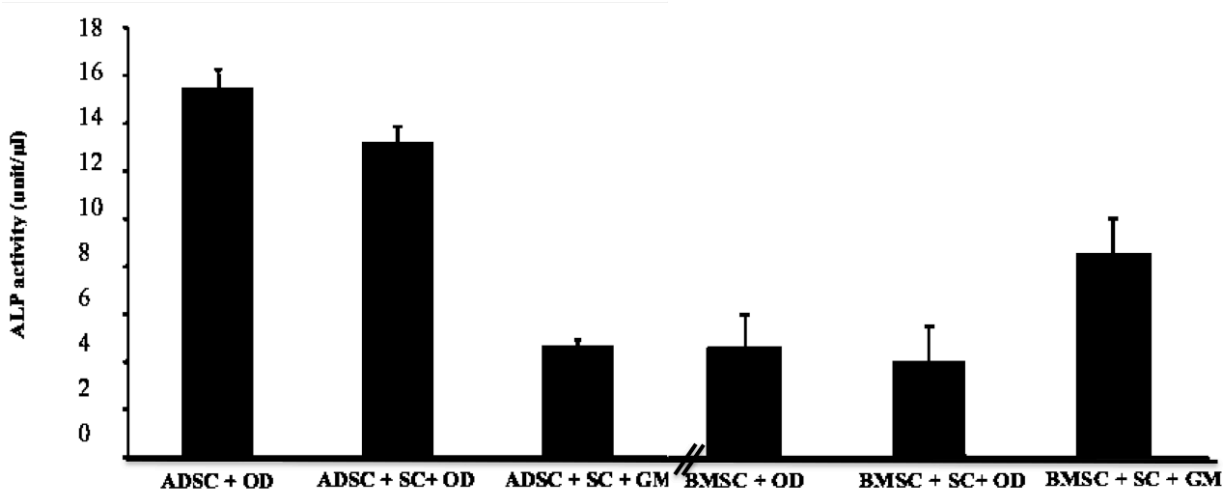

Figure 3.4. Alkaline phosphatase assay: ADSC on left with PEEK scaffold (SC) and osteodifferentiation media (OD) produced more ALP than growth media (GM) alone, but less than ADSCs in OD with SC. BMSC on right show greater differentiation with GM over BMSC with OD with or without scaffolds (N=8).

Cytocompatibility of the scaffolds to MSCs was done via scanning electron microscopy (SEM) to examine for cell adherence After being co-cultured with PEEK scaffolds for 7 – 9 days, cells were analyzed using SEM at magnification of 10000x (**Figure 3.5**).

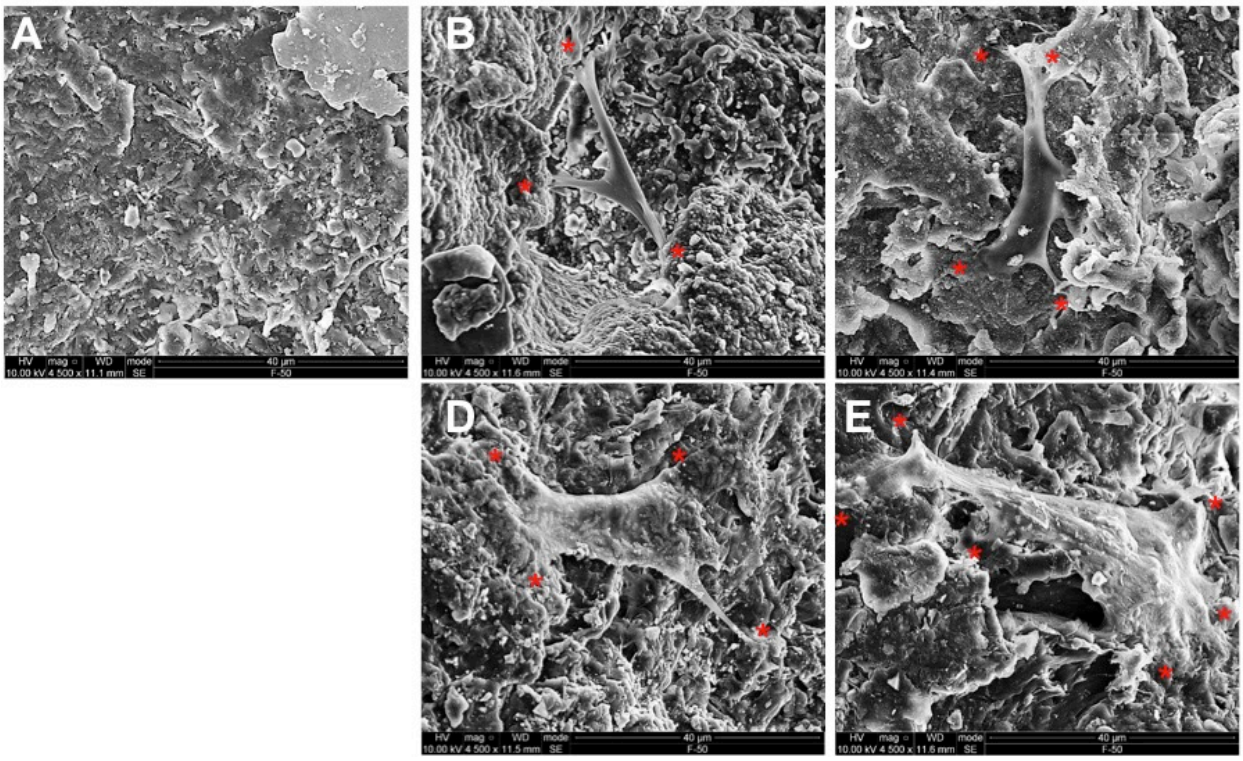

Figure 3.5. Scanning electron microscopy images taken at 10,000 x on day 1 (top row) and day 7 (bottom row) of cell culture with ADSCs (b and d) and BMSCs (c and e) versus the scaffold without cells (a). The stars denote points next to the cells' attachment to the PEEK scaffolds.

As compared to the scaffolds without cells, there is evidence of both ADSC and BMSC filament attachment within the pores of the scaffolds.

3.5 Discussion

Polyetheretherketone is increasingly being used as an alternative to conventional implants, especially in orthopedic applications; however it's use in craniofacial reconstruction is limited by a poor bioactivity and consequent weakened bony-implant fixation. With the emergence of tissue engineering, a field that involves the use of a scaffold, building blocks and nourishment, improved PEEK fixation may be achievable. This study characterizes the combination of an SLS-printed PEEK scaffold, rat mesenchymal stem cells (MSC) as the building blocks and osteogenic

differentiation media as nourishment. We secondarily compare two MSC sources, adipose and bone marrow-derived as a proof of concept before beginning animal trials.

Multiple studies have attempted to modify the final PEEK construct, but few have examined SLS-printed PEEK in combination with cells as a means of promoting adhesion and differentiation. Surface modification via physical or chemical treatments in the post-fabrication phase have been studied. Zhao et al. (13) created sulfonated PEEK with pore size between 0.5-1 micron that supported cell adhesion and viability and Landy et al. (37) determined that a PEEK structure fabricated in an extrusion process with 50% porosity and 100 micron size supported osteoblastic differentiation. These processes require multiple steps, are time consuming and require a specific skillset. SLS produces customized PEEK scaffolds in a one-step, time-effective process. This technique employs a CO_2 laser to fuse a powder-bed of PEEK particles into layers of two-dimensional structures to create a three-dimensional shape.

MicroCT analysis of the printed PEEK scaffolds printed demonstrated a porosity of 36.38 ±6.66 less than the 60% porosity designed using CAD software. This discrepancy may be attributed to the SLS process itself. The EOSINT P800 sinters high performance polymers at temperatures of up to 385°C. Studies have shown that PEEK exhibits superior thermal degradation resistance to various polymers with a decomposition onset temperature of 575°C (38). Despite this, once melted at a temperature of 343°C, we observed that the designed microstructure (pore size and interconnectedness) was not preserved entirely. As such, the majority of the pores were open (35.08%) with only 2.05% being closed. Much of the shrinkage occurred at the center of the sample. Thus, we argue cell penetration into the deeper structures of the scaffolds was severely inhibited. Future studies should account for this “shrinkage” in pore size by increasing the digital file diameter before printing.

Other methods to increase PEEK bioactivity have included impregnation with bioactive materials, either via biocomposite manufacturing or infiltration with stem cells. A common biocomposite of hydroxyapatite and PEEK (HA/PEEK) has been limited by an inability to bear long-term critical loading (39). While studies have investigated the combination of different biomaterials and several osteoprogenitor cells, no study has investigated two sources of MSCs with SLS-printed PEEK.

The results of this study demonstrate that unreinforced SLS printed PEEK, supports both adipose and bone marrow mesenchymal stem cell growth and integration; however, ADSCs differentiated into osteoblasts much more reliably when co-cultured with the scaffolds. This finding is consistent with the literature that supports ADSC growth on PEEK. Waser-Althaus et al. (40) demonstrated that ADSCs grown on oxygen and ammonia plasma-treated PEEK exhibited a doubled mineralized degree relative to the original PEEK. To our knowledge, this is the first study to investigate the interactions of both ADSC and BMSC with PEEK concurrently. The use of MSC is an area of active research for tissue regeneration as they can differentiate into bone, fat, muscle and cartilage under the right biological cues (41). Two major sources of MSCs can be found in adipose tissue and bone marrow. A major difference however between the two is the contrasting methods of extraction, with BMSC isolation causing significant donor site morbidity compared to stromal vascular fraction (SVF) from ADSC (42). As the in vitro results support ADSCs as an ideal candidate for bony tissue engineering using PEEK scaffolding, the future practical implications of performing liposuction over a bone marrow biopsy may facilitate its acceptance going forward.

A limitation of this study includes the sub-optimal porosity and heterogeneity of the scaffolds. Future studies using an ex-vivo model are required to account for the differences from vibration

and mechanical stimulation on bone cells versus that from an in vitro passive model. Implantation of the scaffolds into critical size osseous defects of vertebrate mammals would offer the ability to characterize the PEEK/MSC hybrid as a bone substitute by quantifying the load-bearing dynamic response of bone. Measuring implant fixation, foreign body rejection, tensile and compression strength changes are important parameters to consider when considering a tissue engineered construct alternative. Substituting PEEK in orthopedic applications, such as fracture fixation plates and screws, is described (21); however, PEEK's utility in a craniofacial load-bearing capacity has yet to be established. PEEK/MSC scaffold transplantation into critical size osseous mandibular defects of vertebrate animals would augment the results of this study. The in vitro results support SLS-printed PEEK/MSC scaffolds as a potential alternative to autologous bone for reconstruction. A rabbit model, where size, handling, improved bone regeneration mechanisms and reduced genetic variation provide the optimal parameters for implant analysis is currently being considered for subsequent studies.

3.6 Conclusion

Tissue engineering using a rapid-prototyped PEEK scaffold, adipose MSCs and differentiation media may prove to be a viable alternative to conventional implants or autologous bone used today for craniofacial reconstruction. PEEK can be selectively laser sintered to provide both porosity (for integration) and customizability (for defect reconstruction) that other alloplastic materials and current surgical procedures cannot offer. Increased osteointegration promotes biocompatibility, offers better bony-implant fixation and may afford greater overall strength to provide therapy in load-bearing applications. Future studies are needed to improve the

manufacturing process and examine the biocompatibility of the scaffolds before PEEK/MSCs composites present a promising alternative to implants in craniofacial reconstruction.

3.7 Conflict of interest statement

The authors have no conflicts of interest to declare.

4 Discussion and linking statements

4.1 Linking statement from first manuscript

As the study in the previous manuscript demonstrated, an in vitro comparison of two mesenchymal sources of stem cells demonstrates superiority of differentiation of adipose stem cells when interacting with a 3DP polyetherketone scaffold. This study determined that heating during the SLS process causes pore shrinkage and thus the follow up study accounted for this, increasing the design 25% larger than the desired size.

4.2 Implications

This proof of concept study established the feasibility of co-culturing stem cells with a bioinert polyetherketone plastic. In fact, the addition of PEK to the stem cells accelerated their osteodifferentiation, perhaps providing a physical barrier to spread and consequent paracrine signaling from cell to cell. The ability to harvest adipose cells using liposuction, over the alternative bone marrow cells through bone marrow biopsy, could provide the surgeon with a simpler way of obtaining cells at minimal risk and decreased pain to the patient.

4.3 Limitations of study and linking statements to second manuscript

The major limitation of this study was that it was simply an in vitro study that didn't examine the composite scaffolds interaction with a native vertebrate environment. Additionally, while cells adhered to the scaffold surface, no assessment on bone-implant interface could be done. The second study served to address these points in an animal model.

5 Manuscript 2

Roskies M, Fang D, Abdallah N, et. al (2017). "Three-dimensionally printed PEKK scaffolds with stem cells for the reconstruction of critical-sized mandibular defects". *The Laryngoscope [Epub ahead of print, Aug 4, 2017]*

5.1 Abstract

Objective: Additive manufacturing offers a tailored approach to tissue engineering by providing anatomically precise scaffolds onto which stem cells and growth factors can be supplied. Polyetherketoneketone (PEKK), an ideal candidate biomaterial, is limited by a poor implant-bone interface, but can be functionalized with adipose-derived stem cells (ADSC) to promote integration. This in vivo study examined the interaction of a 3D-printed PEKK/ADSC implant within the critical-sized mandibular defect in a rabbit model.

Study Design/Methods: Twelve trapezoidal porous scaffolds with dimensions of 1.5 x 1.0 x 0.5 cm were printed using selective laser sintering (SLS). ADSCs were seeded on the scaffolds that were then implanted in marginal defects created in New Zealand rabbits. Rabbits were euthanized at 10- and 20-week intervals. Microcomputed tomography (microCT) was used to characterize bone ingrowth and was correlated with histological analysis. Stress testing was performed on the scaffolds before and after implantation.

Results: All scaffolds were well integrated into adjacent bone. Bone-to-tissue volume increased from 30.34% (+/-12.46) to 61.27% (+/-8.24) and trabecular thickness increased from 0.178 mm (+/-0.069) to 0.331 mm (+/-0.0306) in the 10 and 20-week groups, respectively compared to no bone regrowth on the control side ($p<0.05$). Histology confirmed integration at the bone-implant

interface. Biomechanical testing revealed a compressive resistance fifteen times that of bone alone ($p < 0.05$)

Conclusion: 3D-printed PEKK scaffolds combined with ADSCs present a promising solution to improve the bone-implant interface and increase the resistance to forces of mastication after mandibular reconstruction.

5.2 Introduction

Despite major advancements, craniofacial reconstruction with osteocutaneous free flaps subjects patients with significant co-morbidities to longer operative times, multiple operative sites and self-reported decreases in quality of life and cosmetic acceptability (43, 44). Additionally, the degree of emotional impairment following reconstruction of the head and neck correlates to the patient's perception of appearance alteration from their baseline and not to the ideal fashioned by the surgeon (45). Additive manufacturing (commonly known as three-dimensional printing) offers a tailored approach to tissue engineering by providing anatomically precise, patient specific scaffolds onto which stem cells and growth factors can be supplied. Recent work on bone regeneration has focused on biomaterials like natural polymers, ceramics and titanium that are limited by increased cost, weak mechanical properties, extended degradation time, low compressive strength and potential metal ion release (11-13).

One candidate biomaterial for scaffold applications is polyetherketoneketone (PEKK) as it exhibits exceptional biocompatibility and mechanical strength (31). Despite this, its use in mandibular reconstruction has been limited by a poor implant-bone interface and resultant decreased strength. Attempts to "functionalize" polyetherketones via post-hoc structure modification (15, 46) or bioactive material incorporation (47) may prove to be time consuming

and imprecise. Previous work has demonstrated improved bioactivity of polyetherketone scaffolds when embedded with mesenchymal stem cells (MSCs)(48). This in vivo study examines the interaction of custom 3D-printed PEKK scaffolds embedded with adipose-derived mesenchymal stem cells (ADSCs) and cell growth media when implanted in a critical-sized rabbit mandibular defect.

5.3 Materials & Methods

5.3.1 Design, printing and characterization of scaffolds

Computer-aided design (CAD) software (Autodesk Within Medical, version 4, CA, USA) was used to create trapezoidal porous scaffolds with dimensions of 1.5 x 1.0 x 0.5 cm (length, height, width) (**Figure 5.1A)**.

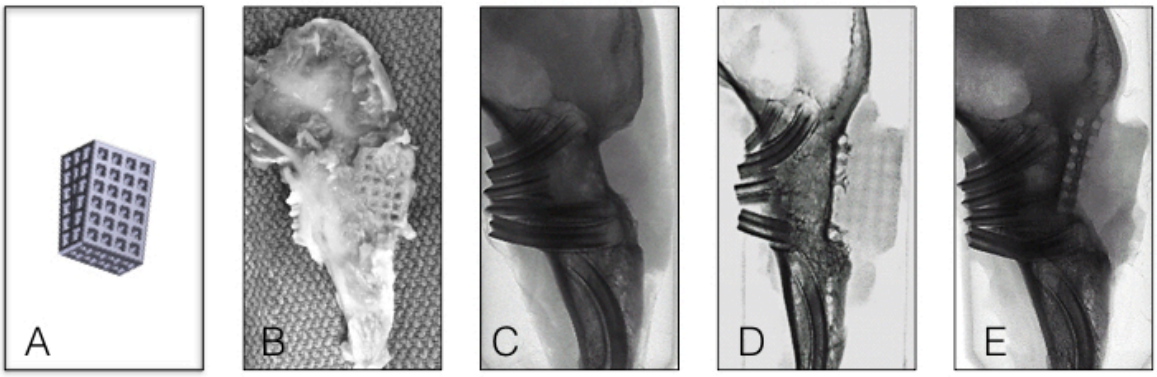

Figure 5.1 (A) Computer-aided design (CAD) image of trapezoidal scaffold with dimensions of 1 x 0.5 x 1.5 cm, strut size of 1 mm, porosity of 50% and pore size of 1000 microns. (B) Photograph of the PEKK/ADSC composite at 10 weeks firmly embedded into adjacent bone. MicroCT images of control group 20 weeks (C), 10 week (D) and 20 week (E) samples.

To overcome a previous limitation of 25% pore shrinkage using the selective laser sintering (SLS) 3D printing process (1), pore size was designed at 1000 microns for a projected ideal size

of 750 microns. The design included a strut size of 1.0 millimeter and porosity of 50%. SLS was used to print eighteen OXPEKK© scaffolds using the EOSINT P800 printer (Oxford Performance Materials, CT, USA). SLS is a precise method of additive manufacturing that employs CO_2 laser to sinter thin layers of PEKK powder together at its melting point in successive two-dimensional slices to create a 3D dimensional solid construct. A high-pressure steam sterilizer (Yamato SM 300, Yamato Scientific, Japan) was used to autoclave the scaffolds (121°F for 12 minutes) prior to cell seeding.

5.3.2 Isolation, expansion and differentiation of rabbit ADSCs

6-8 week old New Zealand female rabbits were used for both the isolation of adipose-derived stem cells and for the experimental model. For isolation, 2 animals were used. Once euthanized, animals were shaved and aseptically washed. Subcutaneous adipose tissue was harvested from the inguinal, neck and back regions and adipose stem cells were isolated according to established protocols (48). Briefly, adipose tissue is digested, centrifuged, suspended, strained and then cultured in a 5% humidified incubator at 37°C for 3 days. Cell culture medium is changed every 2-3 days until cells reach 70-80% confluency. Scaffolds were submerged in a 60 cc syringe with complete culture medium and a negative pressure of 100 kPa was applied while vibration was added to release effervescence for 100 seconds. 2.5 x 10^6 cells were seeded on the scaffold and incubated in a 5% humidified incubator at 37°C.

Osteodifferentiation of ADSCs on six 3D printed PEKK scaffolds was assessed using alkaline phosphatase assay (ALP) in vitro, a biomarker for bone mineralization. After cell seeding on the PEKK scaffolds in a 12-well plate, the two were immersed in osteogenic differentiation media composed of α-MEM, dexamethasone, β-glycerophosphate, 2-mercaptoethanal and

ascorbic acid. Every 2-3 days over a period of 28 days, the media was replaced and cells were examined. After sonication, p-nitrophenyl phosphate tablets were added to the supernatant, which was then incubated for 1 hour. Once a color change was noted, a plate reader (Bio-Tek Instruments, VT, USA) was used to quantify the results.

5.3.3 Surgical procedure and animal care

Approval for all procedures was obtained from our institution's animal ethics review board (approved protocol #2015-7571, www.animalcare.mcgill.ca). All twelve rabbits were acclimatized 14 days in a quiet, clean environment prior to the surgical procedure. Once brought to the operating suite, general anesthesia was induced and they were intubated endotracheally. Animals were prepped and draped for sterility. Depth of anesthesia was confirmed prior to incision using the pedal withdrawal reflex and vital signs were monitored throughout. 2-3 cc of 1% lidocaine with 1:100,000 epinephrine was infiltrated subcutaneously at the incision site. A 2 cm incision was made in the skin and cautery was used to dissect down to the level of the mandible body. Significant efforts were made to ensure the periosteum was removed. Once incised, the periosteum was lifted using a Freer elevator and removed in its entirety. A diamond burr was used to remove the next layer of underlying bone until superficial bleeding was observed. An inferior segment of the body was marked measuring 1.5 cm x 1.0 cm and a diamond burr was used to create the bicortical critical size marginal defect. This was done in the same animal bilaterally to create the experimental (scaffold placed) and control (defect left open) arms of the study. Twelve scaffolds were placed in a predetermined, randomly selected side and stabilized using a musculo-fascial sling. Soft tissue was closed using 4-0 Vicryl sutures in interrupted fashion and skin reapproximated using 5-0 Monocryl in a running subcuticular fashion (**Figure 5.2**).

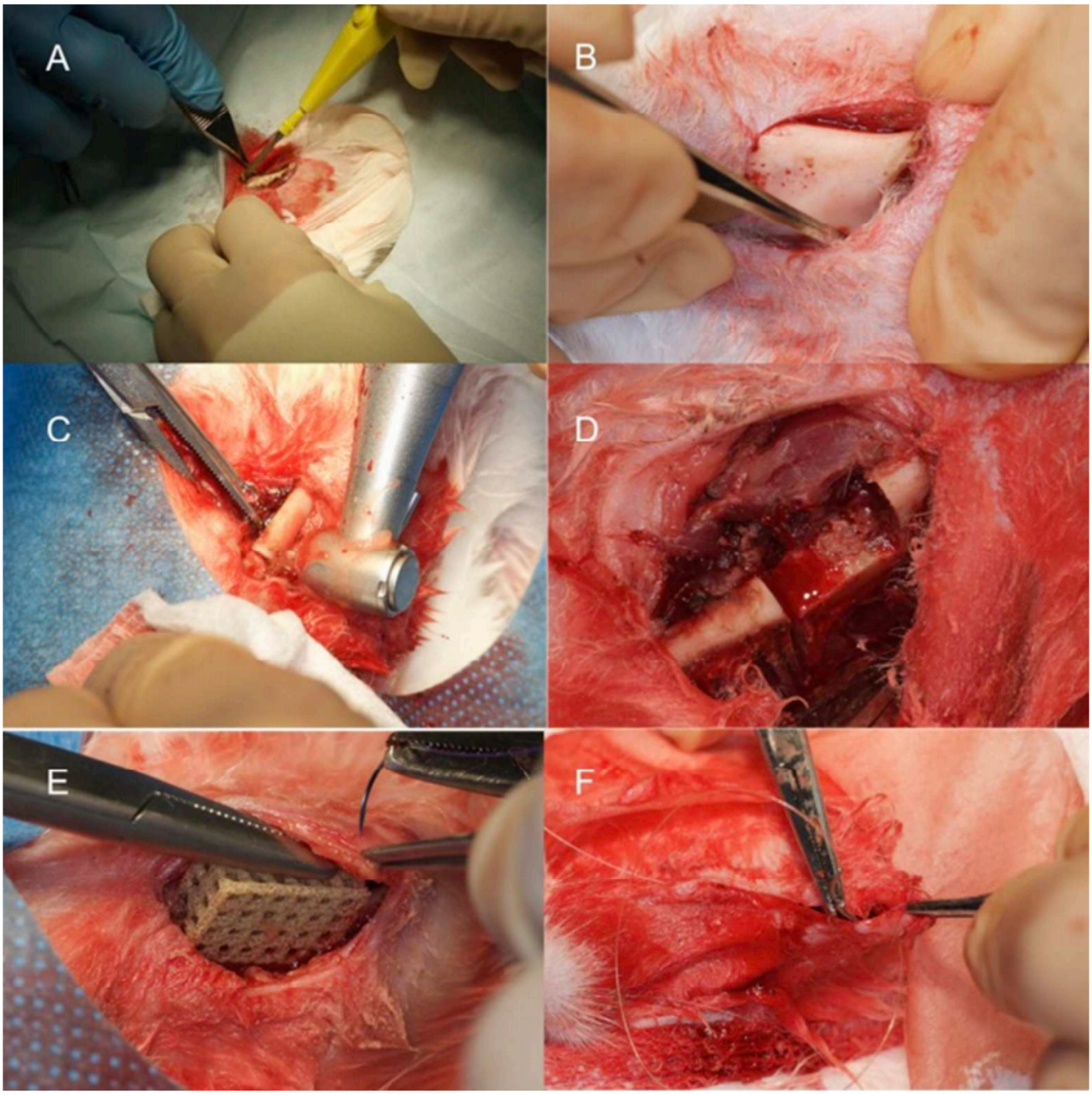

Figure 5.2 Surgical procedure. A) incision B) exposure of mandibular body C) drill bicortical marginal defect D) defect shown E) placement of scaffold F) closure with musculofascial sling.

Post-operatively, animals were placed in a warm environment and analgesics were administered regularly over 72 hours. Daily wound examinations were performed and weight and

hydration status were monitored closely throughout. A soft diet was initially prescribed and transitioned to solid diet as tolerated.

5.3.4 Sacrifice & Macroscopic Assessment

Animals were sacrificed at two periods of 10 and 20 weeks. Upon retrieval of the scaffolds, bone to implant fixation was examined by palpation. Wound healing was assessed and signs of infection or local inflammation were recorded. Each half of the mandible was removed in its entirely. After fixation in 10% formalin, the samples were kept in 70% ethanol at 4°C for 24 hours.

5.3.5 MicroCT, Histology, Stress Testing

Microcomputed tomography (microCT) was used to characterize the bone ingrowth inside the mandibular defects constructs. Scans were performed using a SkyScan 1172 instrument (Bruker-Microct, Kontich, Belgium). The X-ray source was operated at 60 kV/167 l A with a 0.5-mm Al filter. Images were acquired with a rotational step of 0.4°. MicroCT was used to assess for radioopacification within the scaffolds, suggesting either soft tissue, fibrosis or bone integration. In addition, CTAn software (Version 1.13.11, Skyscan, Kontich, Belgium) was used to calculate the bone volume-to-tissue volume (BV/TV) and trabecular thickness of the bone ingrowth inside the mandibular defects.

5.3.6 Histological assessment

Prior to the sectioning, the bone surrounding six implants were trimmed so that ~1cm remained on either sides. This was done to reduce the sample's size to allow for proper processing. With this amount of remaining bone the interfaces could still be evaluated after the sectioning.

Initially the trimmed samples were decalcified with 4.13% of EDTA for ~15-25 days. The decalcification was confirmed by needle puncturing through the bone. Even though the bone was soft, microtome section was not possible because of the PEKK's rigidity. The samples were then embedded in methylmethacrylate (MMA) and sectioned at 5µm with a Polycut S heavy-duty microtome (Reichert-Jung, Leica Instruments GmbH, Germany) equipped with a tungsten carbine knife wedge at a 50° angle. The prepared sections were then stained with Hematoxylin and Eosin as well as Masson-Goldner-Trichrome for the evaluation of osteointegration at the interfaces. Cellular imaging and analysis was performed using Volocity 3D Image Analysis Software ™ (Version 4.5.1) (PerkinElmer, Inc., WA, USA).

5.3.7 Mechanical testing

Six scaffolds were subjected to compressive stresses using a 50 kN force transducer (313 Family Electromechanical Universal Test Machine, Test Resources, MN, USA). Maximum load (N) to fracture at a constant compression speed of 3 mm/min was measured for each sample (PEKK/ADSC) versus the control mandible bone (-PEKK/-ADSC) and PEKK scaffolds alone.

5.3.8 Statistical Analysis

Intergroup differences between experimental and control groups at different time points were compared using ANOVA with Tukey's post-hoc tests (SPSS 11.0). Differences were considered significant at $P < 0.05$.

5.4 Results

Eighteen trapezoid scaffolds were 3D printed using SLS and had average dimensions of 1.49 x 1.04 x 0.57 cm (length x height x width respectively). Porosity was 50% and strut size was 1.02 [0.69 – 1.28]. Pore size averaged 730 microns [0.3 – 1.24]. Alkaline phosphatase activity measured on six scaffolds not subsequently implanted was 0.050 x 10^{-2} (+/-0.002) units for ADSCs, 0.0454 x 10^{-2} (+/-0.102) units for ADSCs with osteodifferentiation media and 0.552 x 10^{-2} (+/-0.1668) units for the PEKK/ADSC composites ($p < 0.05$) (**Figure 5.3**).

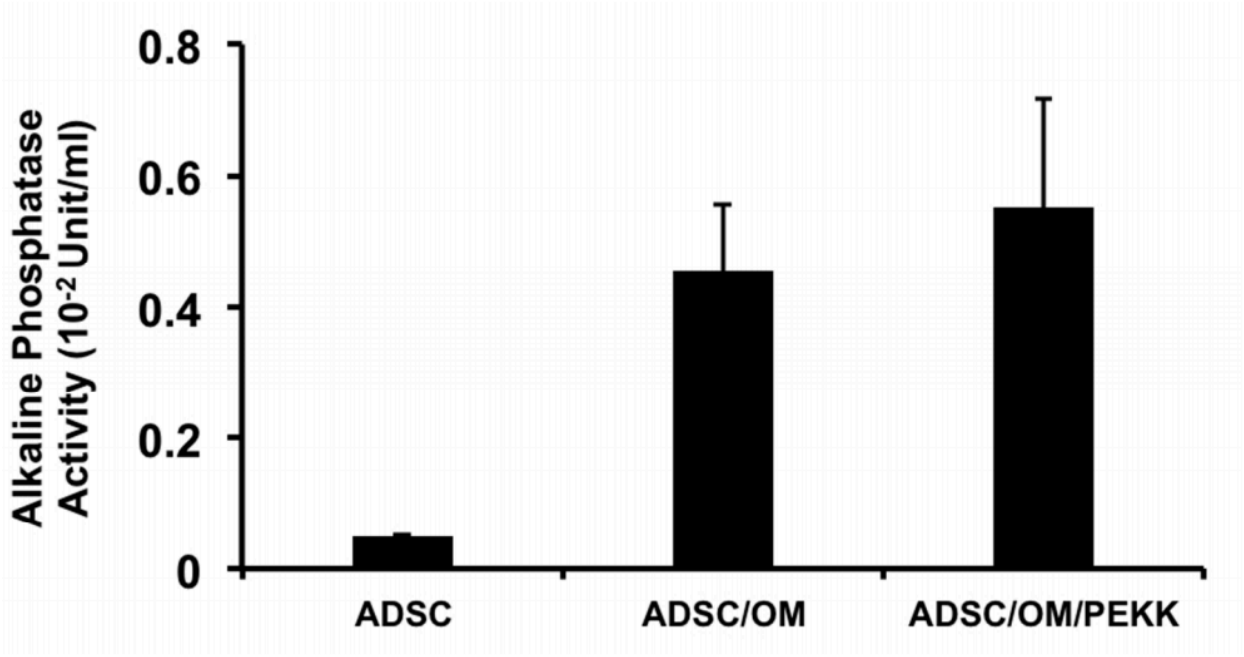

Figure 5.3 Alkaline phosphatase assay. ADSC osteodifferentiation alone in tissue culture plate (ADSC) versus with osteodifferentiation media (ADSC/OM) versus with media and within scaffolds (ADSC/OM/PEKK). (N=6)

The rabbits tolerated the procedure well and all wounds healed appropriately. Exceptions were noted with one minor wound dehiscence that was stapled closed and a subsequent local wound infection resolved without treatment near the study endpoint. The latest day for any animal to resume solid oral diet was post-operative day 7. The average weight gain for the 10-week group

was 0.63 kg [0.35 – 0.9] and for the 20-week was 1.19 kg [0.85 – 1.7]. Through palpation, 100% of scaffolds were firmly embedded into adjacent bone (**Figure 5.1B**).

MicroCT performed at 10 and 20 weeks demonstrated interval radioopacification migration from the superior border of the defect more inferiorly (**Figure 5.1C-E**). Bone volume-to-tissue volume increased from 30.34% (+/-12.46) to 61.27% (+/-8.24) and trabecular thickness increased from 0.178 mm (+/-0.069) to 0.331 mm (+/-0.0306) in the 10- and 20-week groups, respectively ($P<0.05$) (**Figure 5.4**).

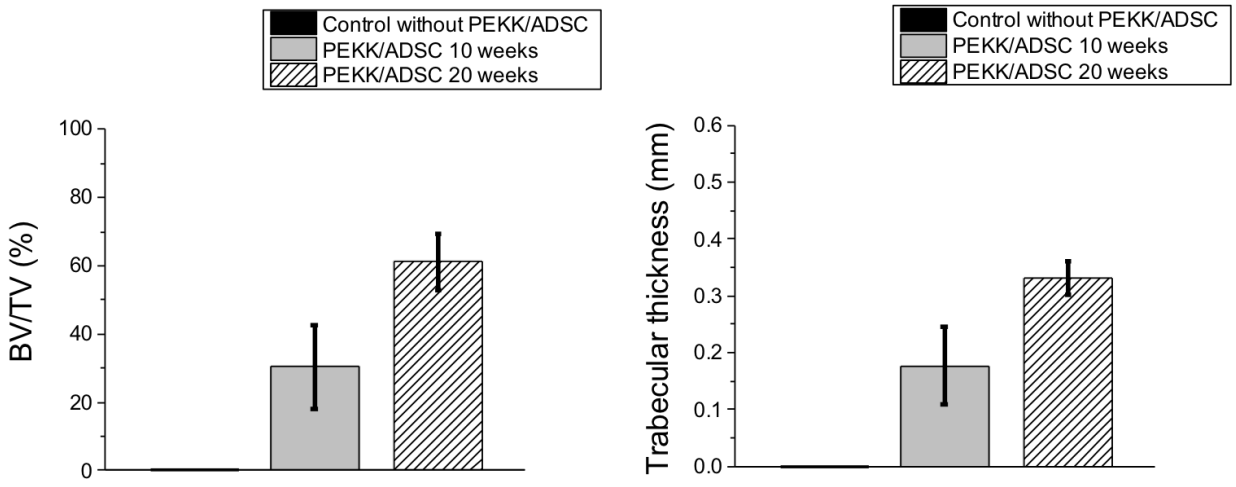

Figure 5.4 Bar charts illustrating the microCT evaluation of bone volume-to-tissue volume (BV/TV) (left) and trabecular thickness (right) of the mandibular defects at 10 weeks and at 20 weeks. Brackets indicate statistical significance at $P<0.05$.

Masson's trichrome demonstrated a mixed of lamellar and woven bone at the bone-implant interface (**Figure 5.5**).

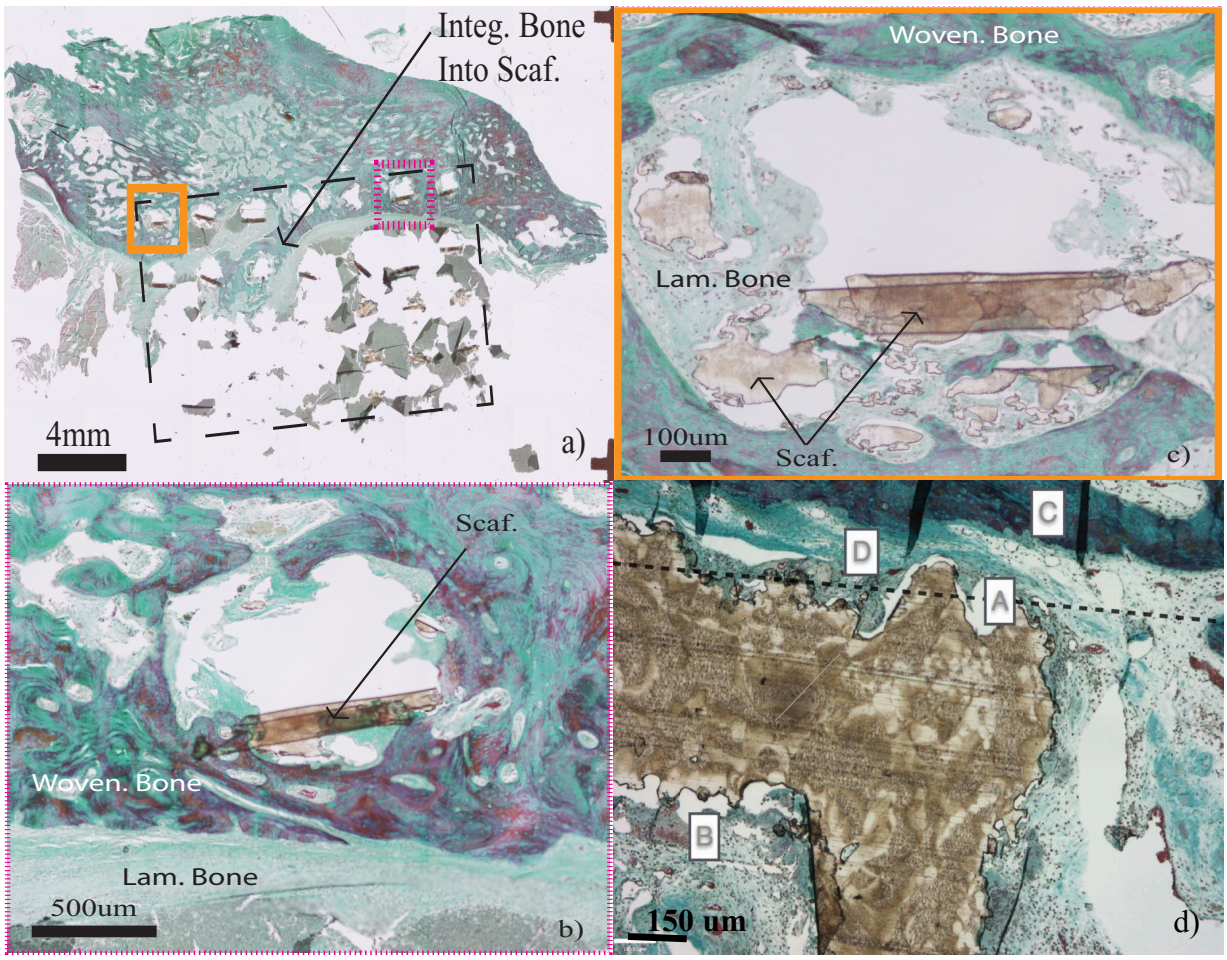

Figure 5.5: Massons Goldner Trichrome stain of a sagittal section taken from the bone implant site 20 weeks post-operative. a) Overview of the entire tissue examined with the ventral side on the bottom and anterior on right. Black long dashed rectangle shows diameter of scaffold. Arrow shows integration of the bone into the scaffold. The smaller squares, dash and full, indicate the location of next two pictures. b) and c) Red and blue stains enter the scaffold pores showing the tissue has interacted with the scaffold. d) bone-scaffold interface at A with mix of woven (C) and lamellar (D) bone. B) shows integration of tissue within scaffold pore again.

Maximum load for rabbit bone explanted from control side (defect without implantation of scaffold) was 500.3 N and for PEKK scaffolds alone (positive control) was 3003.44 N. By contrast, the six PEKK/ADSC composites explanted at 20 weeks averaged 7357.29 N ($P < 0.05$) (**Figure 5.6**).

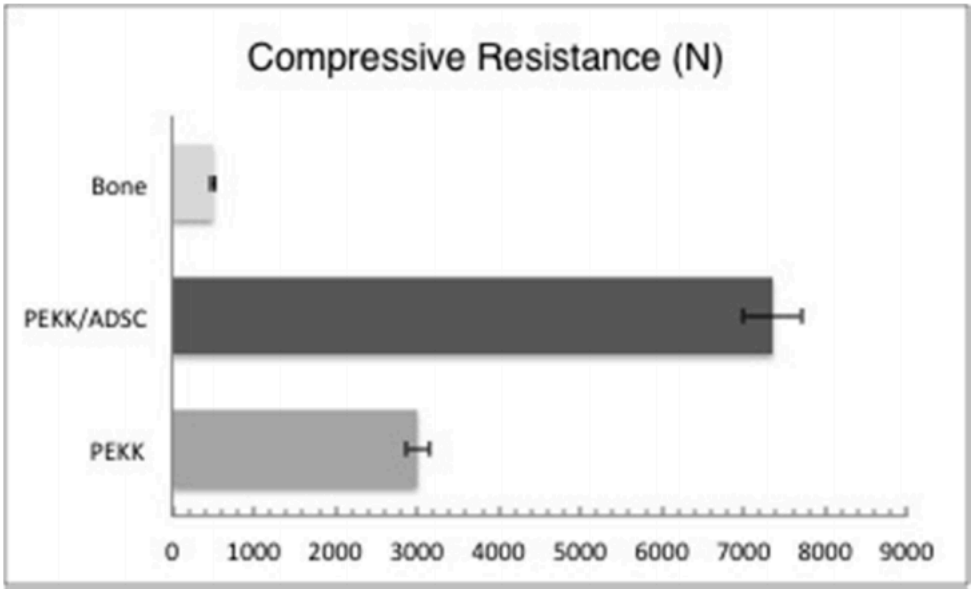

Figure 5.6 Biomechanical stress testing. Resistive capacity of PEKK (non-implanted, no ADSCs) versus PEKK/ADSC composite (explanted at 20 weeks) and bone (negative control) (N = 6, each group).

5.5 Discussion

The gold-standard for reconstruction of critical-sized mandibular defects employs autogenous bone; however, patient, surgeon and healthcare system limitations may preclude candidacy for this operation. Bioactive implants, in the form of trabeculated scaffolds may provide a viable alternative in select cases. 3D printing offers the ability to recreate patient-specific anatomy, thereby improving cosmesis and restoring native function, leading to improved patient and surgeon satisfaction. Several authors have attempted to increase the bioactivity of inertly printed scaffolds, but these processes are time consuming and imprecise.

This in vivo study investigated a 3D-printed PEKK/ADSC composite as an alternative for mandibular reconstruction. PEKK is a thermoplastic material that exhibits exceptional biocompatibility and chemical/thermal stability (31). Additionally, it is radiolucent, an important

characteristic of an implant for the head and neck cancer patient (7). Notably, the OXPEKK© formulation, printed via SLS is FDA approved for implantation and is used in the fields of orthopedic surgery and neurosurgery (FDA 501(k) clearance K142005). The use of polyetherketones in craniofacial reconstruction has been described in the midface region (10), but its use in mandibular reconstruction, where load-bearing strength is required has not been previously investigated.

The authors' previous work has shown that polyetherketones can be "functionalized" with stem cells in order to strengthen the bone-implant interface (48). This process using the SLS/ADSC construct has the advantages of being single stage, extremely precise with the potential for an easy donor cell harvest (i.e. liposuction).

The results from this study indicate that a 3D-printed porous PEKK scaffold can be impregnated with ADSCs and growth media in order to integrate into the mandible of an animal model. Macroscopic, radiologic and histologic assessments confirmed the integration of the PEKK/ADSC composite in rabbit marginal mandibular critical sized defects. Landy et al. (37) determined that a PEEK structure fabricated in an extrusion process with a 50% porosity and 100 micron size supported osteoblastic differentiation; however, more recent studies support larger pore sizes for mesenchymal stem cell differentiation (49). The SLS 3D printing process provided the exact porosity and an anticipated 25% pore size shrinkage from the CAD file design. An in vitro alkaline phosphatase assay performed demonstrated superior differentiation of ADSCs when cultured within the porous scaffold, rather than alone. This is believed to be a result of the interconnected porous network through which cells can migrate and provide paracrine signaling to one another.

Work by Zhang et al. demonstrated callus formation to the through the entire hydroxyapatite/polyamide nanocomposite implant by 12 weeks; however the edge of the mandible was almost completely restored in the control group by 24 weeks. Our surgical procedure involved stripping the periosteal layer off the control group bone, thus interrupting the cortical blood supply. As a result, the relative difference between our experimental and control groups at 20 weeks is greater, demonstrating a relative new bone volume of 22.85 mm^3.

The compressive strength of the PEKK/ADSC composite scaffolds was fifteen-times higher than that of the control cortical bone group. Compared to other scaffolds cited in the literature, it demonstrates superior strength than porous titanium (50), beta-tricalcium phosphate/chitosan (51), tantalum (52), PEEK foam (37), and porous calcium phosphate cement (53) to name a few. Additionally, PEKK is readily available and cheaper and than most alloplastic materials on the market today.

A weakness of this study includes the lack of an experimental arm using only the PEKK scaffolds (without stem cells) as part of the in vivo component. This positive control was included in the biomechanical testing, however, the importance of stem cells in this context may not have been fully addressed without a direct in vivo comparison. Although the negative control in this study represented the clinical gold standard treatment for marginal mandibulectomy of healing by secondary intention (or plating in some cases), future studies including the three arms of composite, scaffold alone and negative control would better address the importance of stem cells as part of this composite implant. Additionally, despite previous experience that indicates cellular attachment to scaffolds at 28 days(48), cellular "washout" during the surgical procedure introduced the uncertainty of adequate cell density after implantation. A future study using hydrogels or foams would bypass this concern.

5.6 Conclusions

As medicine trends toward patient-centered care, the demand to adapt therapy on a case-by-case basis is ever increasing. To match form with function, additive manufacturing can restore patients' native anatomy. PEKK/ADSC composite scaffolds are a viable alternative to conventional reconstruction for the mandible as they demonstrate favorable bioactivity, biocompatibility and biomechanical strength.

5.7 Conflict of interest statement

The authors have no conflicts of interest to declare.

6 Linking statements to book chapter

The details of many of the experiments performed were too numerous to include in manuscripts; however the step-by-step procedures were compiled for a book chapter. Cell culture, 3D printing, surgical intervention and microCT procedures are outlined below. It lists the equipment required and outlines in a linear fashion the steps needed to perform similar experiments in the future.

7 Book chapter

Fang D, **Roskies M**, Abdallah MN, Bakkar M, Jordan J, Lin LC, Tamimi F, Tran SD. "Three-dimensional printed scaffolds with multipotent mesenchymal stromal cells for rabbit mandibular reconstruction and engineering". *Methods Mol Biol*. 2017;1553:273-291.

7.1 Abstract

Multipotent mesenchymal stromal cells (MSC) derived from both the bone marrow and adipose tissue possess the ability to differentiate into multiple cell lineages, regulate the immune function by secreting numerous bioactive paracrine factors, and hold great potential in cell therapy and tissue engineering. When combined with three-dimensional (3D) scaffolds, MSC can be used for bone defect reconstruction and engineering. This protocol describes the isolation of bone marrow mesenchymal stromal cells (BMMSC) and adipose-tissue derived stem cells (ADSC) from rabbits for subsequent seeding on tissue-engineered 3D-printed scaffolds and transplantation into a rabbit-model with the goal of repairing large osseous mandibular defects (one quarter of the lower jaw is removed surgically). Steps to demonstrate the three cell differentiation lineage potentials of BMMSC and ADSC into osteocytes, adipocytes and chondrocytes are described. A modified cell seeding method using syringes on scaffold is detailed. Creating a large mandibular bone defect, the rapid prototyping method to print a customized 3D-scaffold, the scaffold implantation procedure in rabbits, and microcomputed tomography (mico-CT) analysis are also described.

7.2 Introduction

The mandible is critical for the facial appearance/ harmony and functions, such as mastication, swallowing and speech ***(54)***. Mandibular defects result from trauma, infections, or after surgical resection of tumors ***(55)***. Autogenous vascularised bone grafts, such as fibular free flaps ***(56)*** or iliac flaps ***(57)***, are most commonly used to reconstruct the mandible, since they offer several advantages, including consistent shape, sufficient blood supply, ample length and low donor-site morbidity. However, autogenous bone harvesting is often associated with a number of complications, including infection, haematoma, fracture and nerve injury ***(57)***. Additionally, thin fibula has proven a poor match for mandibular height, leading to a potential loosening of dental implants.

Recent studies suggest that scaffold biomaterials can be used as alternative materials to reconstruct critical-size bone defect ***(58)***. Three-dimensional (3D) printed scaffolds can be customized and precisely printed based on the CT or MRI 3D picture files of patients. However, it was reported that osteogenesis only occurred in the outer surface of large scaffolds, leading to a non-homogenous distribution of cells ***(58)***. To overcome these limitations, mesenchymal stromal cells (MSCs) were seeded in porous scaffolds and were tested for the reconstruction of bone defects ***(59,60)***.

MSCs derived from both bone marrow ***(61,62)*** and adipose tissue ***(63-65)*** have a great potential in cell therapy and tissue engineering, since they possess the ability to differentiate into multiple cell lineages, and regulate immune function by secreting numerous bioactive paracrine. Bone marrow mesenchymal stromal cells (BMMSCs) have demonstrated osteogenic differentiation both *in vitro* and *in vivo*. So far, bone marrow is considered as the major source of MSCs used for bone engineering applications ***(60,61)***. Compared to bone marrow, adipose tissues

are easier to harvest and are considered as a more practical alternative source for MSCs. Indeed, some studies used a combination of adipose tissue-derived mesenchymal stromal cells (ADSCs) and scaffolds for bone defect reconstruction ***(66,67)***. Moreover, scaffolds loaded with MSCs showed greater osteogenic capacity than the scaffold alone in large animal model ***(68,69)***.

In this chapter, we describe a protocol that uses three dimensional (3D) scaffolds seeded with MSCs derived from either the bone marrow or from the adipose tissue of a rabbit to reconstruct large mandibular bone defects. The rabbit is a preferred animal model for studying mandibular bone repair because rabbits return to normal function within a few days of surgery, have mandibles large enough for creating critical-size defects, and are relatively small for housing and handling ***(58)***. This protocol also describes a modified method for seeding a high density of cells into scaffolds. It has been suggested that cell seeding density in the scaffold is critical for bone engineering ***(70)***, and a higher cell number promotes a higher cell proliferation rate and osteogenic differentiation potential ***(71)***. Therefore, we combined three major cell seeding systems together (low-pressure system, pipette system and syringe system) to achieve a higher cell seeding density by efficiently removing the air bubble entrapped inside the scaffold. In addition, this chapter includes the surgical steps for creating critical-size mandibular defects, scaffold implantation and microcomputed tomography (mico-CT) analysis.

7.3 Materials

7.3.1 Animals

1. 6-8 weeks old New Zealand male rabbits can be used for the isolation of bone marrow-derived mesenchymal stromal cells (BMMSC) and adipose tissue-derived stem cells (ADSC).

2. Adult New Zealand female rabbits (age: 12 months old; weight: 2.5-3.5kg) can be used as recipient animals. All animals are kept under clean condition and provided with food and water in the animal resource center.

7.3.2 Isolation and culture of bone marrow mesenchymal stromal cells (BMMSC)

1. Sodium pentobarbital.
2. 70% ethanol in distilled water.
3. Sterile surgical instruments including sharp straight scissors, forceps and scalpels.
4. Washing buffer: Phosphate-Buffered Saline (PBS) with 5% antibiotic-antimycotic
5. Flushing buffer: alpha Minimum Essential Medium (α-MEM) with 2% antibiotic-antimycotic.
6. 100 mm Tissue culture dish.
7. 2 mL, 5 mL and 10 mL sterile pipettes.
8. Pipette-aid.
9. 5 mL syringe and 21G needle.
10. 70 um cell strainer.
11. 50 mL conical tube.
12. Trypan blue stain 0.4%.
13. Neubauer counting chamber.
14. T-75 tissue culture flasks.
15. Complete culture medium: alpha Minimum Essential Medium (α-MEM), 10% FBS, 1% antibiotic-antimycotic, 1% L-Glutamine.

7.3.3 Isolation and culture of adipose tissue-derived stem cells (ADSC).

1. Sterile surgical instruments including sharp straight scissors, forceps and scalpels.

2. Washing buffer: Phosphate-Buffered Saline (PBS) with 5% antibiotic-antimycotic.
3. Digestive buffer: 0.075% Collagenase type I in PBS with 2% antibiotic-antimycotic.
4. Red Blood Cell Lysis Buffer.
5. 100 mm tissue culture dish.
6. 70 um cell strainer.
7. 50 mL conical tube.
8. Complete culture medium: alpha Minimum Essential Medium (α-MEM), 10% FBS, 1% antibiotic-antimycotic, 1% L-Glutamine.

7.3.4 Multilineage differentiation of BMMSC and ADSC

7.3.4a Osteogenic Differentiation

1. Osteoblast differentiation medium: α-MEM, 1% antibiotic-antimycotic (100 U/mL penicillin-G, 100 μg/mL streptomycin and 0.25μg/mL Amphotericin B), supplemented with 10% FBS, 0.1mM ascorbic acid, and 10^{-8} M dexamethasone, 2 mM β-glycerophosphate.
2. Alizarin Red S solution: 1% Alizarin red S in distilled water.
3. 70% ethanol.
4. PBS.
5. Distilled water.

7.3.4b Adipogenic Differentiation

1. Adipogenic differentiation medium: α-MEM, 1% antibiotic-antimycotic, 10^{-8} M dexamethasone, 10 μg/mL insulin, 0.5 mM 1-Methyl- 3 – Isobutylxanthine (IBMX), 0.5 μM hydrocortisone, 60 μM Indomethacin.

2. Oil Red O stain: 0.3% oil red O staining solution. 0.3 g oil red O (ICN Biomedicals) stain dissolved in 100 mL isopropanol.
3. PBS.
4. 10% Neutral Buffered Formalin.
5. 60% Isopropanol.
6. Distilled water.

7.3.4c Chondrogenic Differentiation

1. 15 mL conical tubes.
2. Chondrogenic differentiation medium: DMEM (4.5g/l Glucose), 1% antibiotic-antimycotic, 10% ITS+Premix Tissue Culture Supplement, 10^{-7} dexamethasone, 1 μM ascorbate-2-phosphate, 1% sodium pyruvate, and 10 ng/mL transforming growth factor-beta 1 (TGF-β1).
3. Anti-Collagen II antibody.

7.3.5 Cell seeding on three-dimensional (3D) scaffold

1. 12-well plate.
2. 0.25% Trypsin-EDTA.
3. Three-dimensional (3D) scaffold.
4. 60 mL syringe.
5. Sterilized tweezers.
6. Air pump.

7.3.6 Transplantation surgery

1. Sterile and sanitized surgical area.
2. Hand washing area.

3. Surgical attire: clean scrubs, masks, bonnets, sterile gloves/gowns.
4. Instrument sterilizer, adequate ventilation hood.
5. Buprenorphine 0.05 mg/kg subcutaneous, ketamine 20-25 mg/kg intramuscular and fentanyl 12.5 mcg/hour transdermal patch as analgesic (*see* **Note 1**).
6. Isoflurane 2% inhalant, Xylazine 5mg/kg intramuscular and Acepromazine 0.75 mg/kg intramuscular for anesthetic.
7. Cefazolin 12 mg/kg intravenous as antibiotic.
8. 1% Xylocaine with epinephrine used as local anesthesia.
9. 20-27 gauge needle.
10. Animal restraint and tissue retraction systems adaptable to animal size.
11. External heat source(s) (e.g. Recirculating water blanket, microwaveable heating packs, or self-regulating heating pad).
12. Ophthalmic ointment (lubricant).
13. Topical antiseptic soap, sterile saline, water and/or 70% ethanol.
14. Hair removal blade, shaver.
15. Initial incision: Surgical blade (#11, #15).
16. Monopolar cautery.
17. Clamp or dissector (e.g. Mosquito clamp, McCabe facial nerve dissector).
18. Forceps.
19. Round diamond bur size#4 with high-speed handpiece.
20. Irrigation with saline.
21. Needle driver (e.g. Mayo-Heagar, Crile-Wood, etc.).
22. Absorbable suture material (e.g. 4-0 Vicryl, 5-0 Monocryl).

23. Scissors.
24. Sterile, clean cages for post-surgery recovery.
25. Tissue harvesting: scissors, low-speed engine.
26. Micro-computed tomography (micro-CT) for 3D analysis

7.3.7 Micro-computer tomography (micro-CT) analysis

1. Micro-CT scanner (*see* **Note 2**).
2. Computing equipment for image reconstruction.
3. Sample holders (e.g. cylindrical vials from the manufacturer, polystyrene tubes, pipette tips, styrofoams).
4. 4% formalin in phosphate-buffered saline (PBS).
5. 70% ethanol.
6. Parafilm® or any other plastic material not containing chloride (if scanning is performed in air).

7.4 Methods

7.4.1 Isolation and selection of bone marrow-derived mesenchymal stromal cells (BMMSC)

1. Euthanize rabbits by an overdose of Sodium Pentobarbital (*see* **Note 3**).
2. Shave and wash legs of rabbit by 70% ethanol.
3. Incise and peel skin to expose the hind limb. Use sterile sharp scissors to cut the joints and remove the muscles and ligaments.
4. Remove femur and tibia at the knee and ankle joints and place in cold washing buffer (PBS with 5% anti-anti) (*see* **Note 4**).
5. Wash bones for 5 minutes x 3 times in washing buffer.

6. Cut the ends of bones to expose the bone marrow. Flush out the marrow plug with a 21G needle attached to a 5 mL syringe filled with flushing buffer.
7. Drawing flushing buffer and marrow plugs up and down several times to make a single cell suspension.
8. Transfer cell suspension through a 70µm cell strainer placed on top of a 50 mL conical tube.
9. Centrifuge at 300 x *g* for 5 minutes at 4℃ and discard the supernatant. Cell pellet is resuspended in the complete culture medium.
10. 50 x 10^6 cells are seeded in a T-75 cell culture flask and incubated at 37℃ in a 5% humidified incubator.
11. After 3 days, remove floating cells by washing with PBS and add fresh culture medium. Change half of the medium every 2-3 days until the cells get to a 70-80% confluency.

7.4.2 Isolation of adipose tissue-derived stem cells (ADSC)

1. Euthanize rabbits by an overdose of Sodium Pentobarbital (*see* **Note 3**).
2. Shave and wash inguinal region, neck and back region of rabbit by 70% ethanol.
3. After incising the skin, subcutaneous adipose tissues at inguinal region and neck and back region are removed and put in cold washing buffer.
4. Wash tissues for 5 minutes x 3 times in washing buffer.
5. After removing the debris, adipose tissues are placed in the tissue culture dish with around 2 mL digestive buffer.
6. Mince the tissues into small pieces with sterile sharp scissors and pipette up and down several times with a 25 mL pipette to further facilitate the digestion.

7. Transfer tissues to a new 50 mL conical tube, add more digestive buffer (1:1, buffer: adipose tissue).
8. Incubate the tissue on a shaker for 30 min at 37℃ in a 5% humidified incubator.
9. Neutralize the collagenase type I with the same amount of alpha MEM containing 20% FBS.
10. Shake the tube vigorously several times to further disintegrate the aggregate of adipose tissue.
11. Centrifuge the sample for 5 min at 800 x *g*, 4℃.
12. Take out the sample from the centrifuge and shake it vigorously to disrupt the cell pellet. Repeat the centrifugation step.
13. Pour out (discard) the adipocytes layer and supernatant containing the collagenase type I without disturbing the cell pellet.
14. Resuspend the cell pellet in 1 mL RBC lysis buffer, and incubate for 10 min on top of ice.
15. Wash with 20 mL of PBS with 2% antibiotics-antimycotics and centrifuge at 800 x *g* for 5 min.
16. Discard the supernatant and resuspend the cells in complete culture medium.
17. Filter cell suspension through a 70 μm cell strainer. Wash the cell strainer with additional 2 mL culture medium to obtain any additional cells.
18. Seed cells in a proper tissue culture plate and incubated at 37℃ in a 5% humidified incubator.
19. After 3 days, floating cells are removed by washing with PBS and add fresh culture medium. Change half of the culture medium every 2-3 days until the cells reach a 70-80% confluency.

7.4.3 Multilineage differentiation of BMMSC and ADSC

7.4.3a Osteogenic differentiation

1. Seed cells in 6-well plate with growth medium and incubated at 37℃ until they reach approximately 50-70%.
2. Aspirate the growth medium and replace with 2 mL of osteogenic-inductive medium per well.
3. Incubate the cells at 37℃ in a 5% humidified incubator and change medium every 2-3 days.
4. After 3 weeks induction, osteogenic differentiation is visualised by Alizarin Red S staining (*see* **Figure 7b**).

7.4.3b Adipogenic differentiation

1. Cells are seeded in 6-well plate with growth medium and incubated at 37℃ until they reach approximately 90-100% confluency. It takes approximately 1-4 days.
2. Aspirate the growth medium and replace with 2 mL of adipogenic inductive medium per well.
3. Incubate the cells at 37℃ in a 5% humidified incubator and change medium every 2-3 days.
4. After 3 weeks induction, adipogenic differentiation is visualised by Oil Red O staining (*see* **Figure 7.11a**).

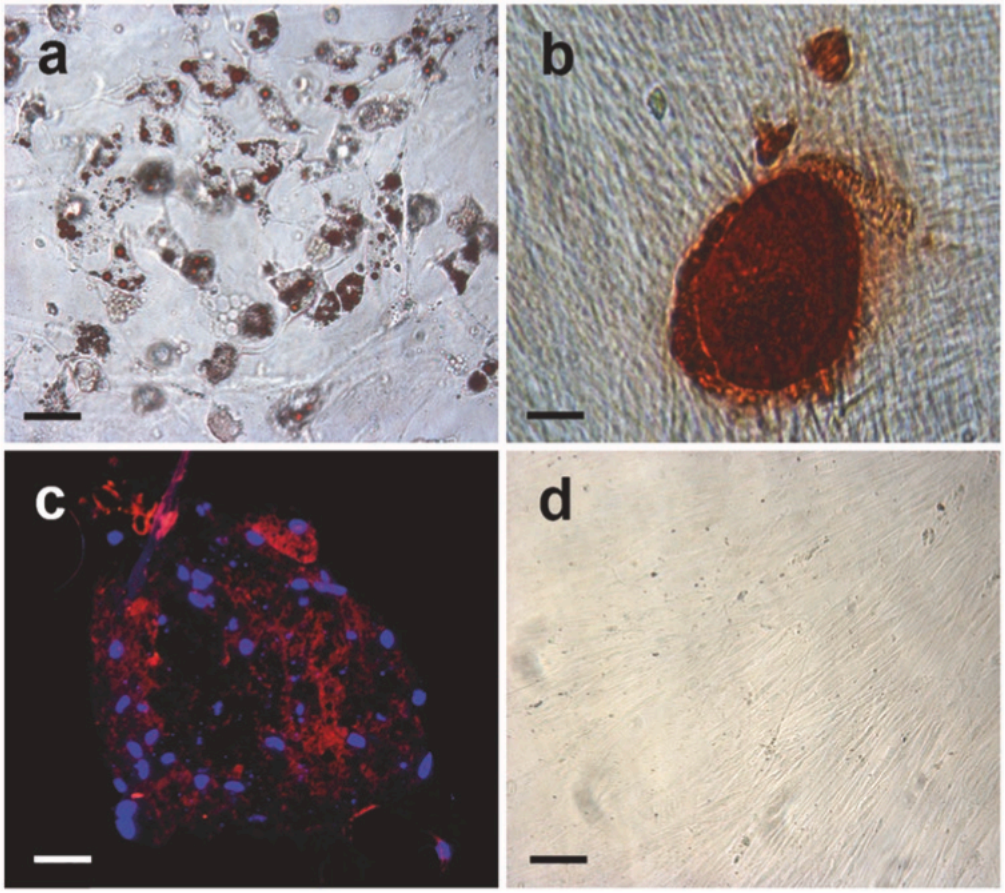

Figure 7.1. Multilineage differentiation of rabbit adipose tissue-derived stem cell (ADSC). *(a) Oil red staining for adipogenic differentiation. (b) Alizarin Red staining for osteogenic differentiation. (c) Collagen type II immunofluorescent staining (in red) for chondrogenic differentiation; cell nuclei are stained in blue. (d) Rabbit ADSCs with growth medium. Scale bar = 38 µm.*

7.4.3c Chondrogenic differentiation

1. 5 x 10^5 cells are resuspended with 5 mL growth medium in a 15-mL conical tube.
2. Centrifuge the cells at 200 x *g* for 5 min at room temperature. Discard the supernatant and resuspend the cells with 0.5 mL chondrogenic differentiation medium.
3. Centrifuge the cells at 200 x *g* for 5 min at room temperature. Do not remove the medium. Loose the cap of the tube to allow gas exchange, incubate upright at 37℃ in a 5% humidified incubator (*see* **Note 5**).

4. Change medium carefully every 2-3 days. Ensure the cell ball is released from the wall of tube and float freely (*see* **Note 6**).
5. Chondrogenic cell pellets are harvested after 14-28 days in culture.
6. Cell pellets are cryopreserved and sectioned into 5-8 μm.
7. Chondrogenic differentiation is assessed by immunofluorescent staining for collagen type II (*see* **Figure 7.1c**).

7.4.4 High cell density seeding on 3-D scaffold (see Figure 3.2)

1. Aspirate all cell growth medium and wash the cell monolayer twice with 37℃ PBS to remove any residual FBS (*see* **Note 7**).
2. Add enough pre-warmed 0.25% Trypsin-EDTA to cover the cell layer.
3. Incubate the cells for 2 min at 37℃. Tap the bottom gently to dislodge the cells.
4. Add the same amount of complete medium to neutralize the Trypsin. Gently rinse the cell layer several times with a pipette to detach all cells.
5. Transfer the cell solution to a new 15 mL or 50 mL conical tube.
6. Centrifuge the cells at 300 x *g* for 5 min at 4℃. Remove the supernatant and resuspend the cell pellet in complete culture medium.
7. Place autoclaved scaffolds in a 60 mL syringe and aspirate 20-30 mL complete culture medium.
8. Connect syringe to the air pump.
9. Turn on the pump and hold the syringe plunger to create a negative pressure.
10. Tap the syringe barrel gently to free the air bubbles trapped in the scaffold.
11. Transfer scaffolds to 12-well plate with sterile tweezer.

12. 2.5 x 10^6 cells are seeded on the scaffold and incubated at 37℃ in a 5% humidified incubator (*see* **Note 8**).
13. After 3-5 days, scaffolds with cells are ready for the transplantation.

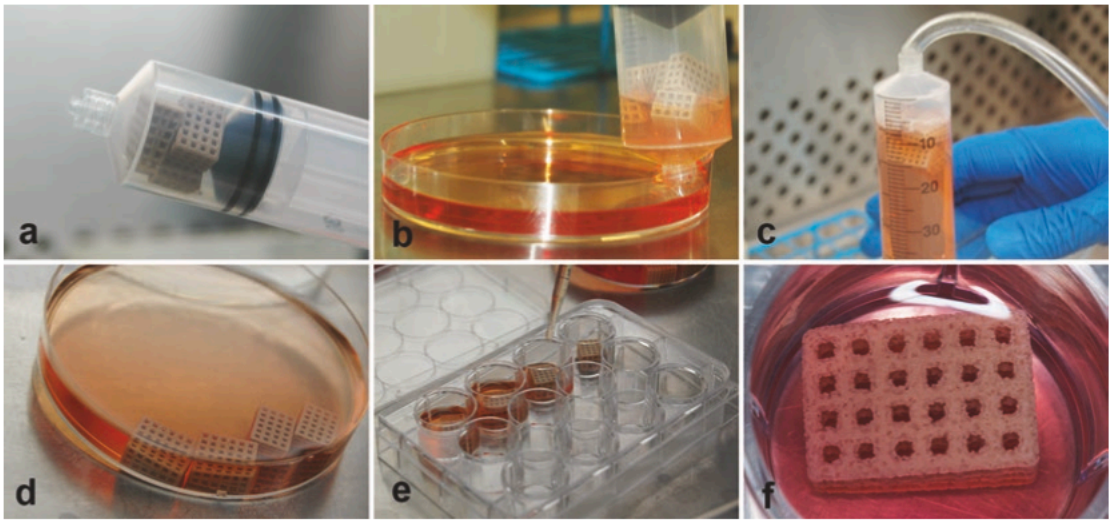

Figure 7.2: Procedures for cell seeding on 3-D scaffolds. *(a and b) Place autoclaved scaffolds in a 60 mL syringe and aspirate 20-30 mL of complete culture medium. (c) Connect syringe to the air pump to remove the air bubbles entrapped in the scaffold. (d) Transfer scaffolds to a 12-well plate with sterile tweezer. (e and f) 2.5 x 10^6 cells are seeded on each scaffold and incubated at 37°C in a 5% humidified incubator.*

7.4.5 Transplantation Surgery

7.4.5a Preoperative surgery preparation

1. Rabbit acclimation of 7-14 days in the animal centre is strongly recommended for their maximal adjustment prior to the surgery.
2. Place animals in appropriate housing soon after their arrival.
3. Surgeon and surgical assistants wear clean scrubs, shoe covers, masks, bonnets with sterile gown/gloves.
4. Observers wear clean scrubs, show covers, masks and bonnets.

5. All instruments are sterilized prior to surgery.
6. Clean instruments before sterilization to remove organic material.
7. Wrap instruments in peel packs, include sterilization indicator.
8. Achieve sterilization by autoclaving (steam), or gas sterilization with ethylene oxide.

7.4.5b Anesthesia, intubation and antiseptic preparation

1. Animals anesthetized in area designated for surgical preparation.
2. Anesthetize the animal: Burprenorphine 0.05 mg/kg given subcutaneously 30 minutes preoperatively. Xylazine-Acepromazine 5mg/kg, and 0.75 mg/kg given intramuscularly during induction.
3. Anesthesia maintained with Isoflurane 2% inhaled via the endotracheal tube.
4. Place animals in prone position with neck extended and mouth facing upwards.
5. 30 mm I.D. endotracheal tube is placed in mouth and advanced until vapor from lungs observed in tube.
6. Once endotracheal tube is placed, auscultation of both lung bases is performed to confirm proper tube placement.
7. Fix tube at 10 centimeters to the mouth using cling wrapped around the nape of the neck.
8. Animal is placed in supine position with a shoulder roll (i.e. wrapped sterile towel).
9. Sterile ophthalmic ointment is applied to both eyes to prevent corneal desiccation and abrasion.
10. Shave the surgical site twice the size of the expected field with an electric razor. Remove all loose hair and debris from the animal using tape.

11. Antiseptic skin preparation: Use aseptic technique when performing skin antisepsis. Start at the centre of the site and move in a circular motion. Perform three scrubs using an antiseptic soap and gauze (e.g. povidone-iodine solution or 2% chlorhexidine solution).
12. Sterile surgical draping: Drape the animal with a sterile, impermeable covering to isolate the disinfected area. Fix the drape in place with tape or clamps. Cover a stand with sterile drape for placement of sterile instruments.
13. Confirm depth of anesthesia before operating with pedal withdrawal reflex and vital signs.

7.4.5c Surgical procedures and monitoring

1. Maintain aseptic conditions during all procedures.
2. Continuously monitor heart rate and rhythm, blood pressure, respiratory rate and depth and temperature and document every 10 minutes.
3. Inject locally 2-3 mL of 1% Xylocaine with epinephrine. The injection depth is to the area of the planned incision.
4. 2 cm incision made superficially in the skin over the inferior border of the mandible (*see* **Figure 7.3b**).
5. Dissection to the level of the mandible (*see* **Figure 7.3c, d & e**). Combination of monopolar cautery and careful dissection using clamp and forceps. Dissect through the masseter muscle. Expose body of the mandible using the back of the forceps.
6. Critical size defect created (*see* **Figure 7.3f and 7.3g**): Target defect creation in body of mandible inferior to the tooth roots. Initiate access with round diamond bur size #4 to outline 1.5 cm by 1.0 cm rectangular marginal defect at the inferior border of the mandible. Complete the bicortical defect using the same bur.
7. Insert and stabilize scaffold with resorbable suture to surrounding soft tissue (*see* **Fig 7.3h**).

8. Closure: Reposition the muscle and parotid gland using resorbable suture (i.e. 4-0 Vicryl) (*see* **Figure 7.3i**). Reapproximate the skin using a 5-0 Monocryl suture in a running subcuticular fashion.

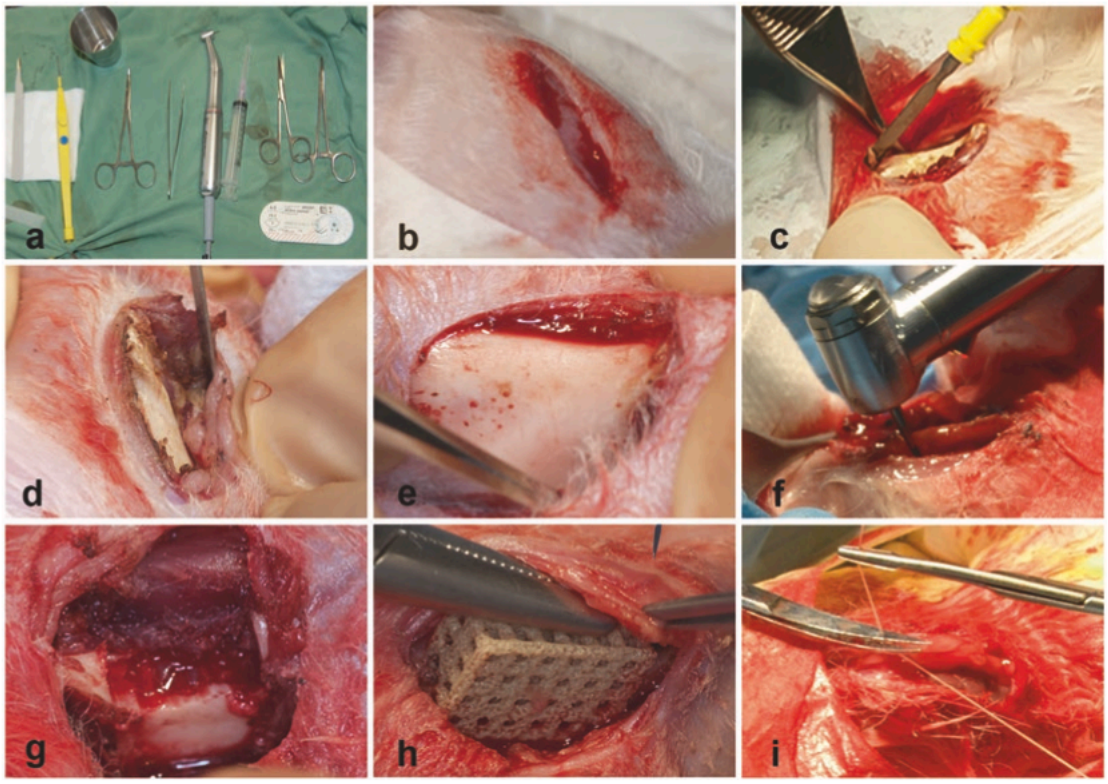

Figure 7.3: Procedures for creating a critical size bone defect on rabbit mandibles and transplantation of the scaffold seeded with MSC. *(a) Surgical instruments. (b) 2 cm incision made superficially in the skin over the inferior border of the mandible. (c, d & e) Dissection to the level of the mandible. (f and g) Critical size defect created (1.5cm*1.0cm). (h) Insert and stabilize the scaffold with resorbable sutures to surrounding soft tissues. (i) Reposition the muscle and parotid gland using resorbable sutures.*

7.4.5d Postoperative care

1. Place animals in a clean, quiet environment for anesthetic recovery until they can maintain a patent airway and sternal recumbency.

2. Keep animal in a warm and dry environment with water circulated heating pad, air circulating heating blanket or surgical thermal barrier.
3. Administer analgesics post-surgically and for the next 72 hours. Buprenorphine 0.02-0.05 mg/kg subcutaneously every 8-12 hours. Avoid non-steroidal anti-inflammatory drugs which may inhibit bone formation.
4. Examine the wound daily until completely healed. It usually takes 3 to 5 days for the wound healing of skin.
5. Monitor weights daily for the first week and assess hydration status clinically (e.g. Energy, vital signs).

7.4.6 Micro-CT analysis (see Note 9)

Micro-CT involves obtaining a sequence of X-ray images of a particular sample at different rotations, and then using computer algorithms to reconstruct a 3D image. The micro-CT procedures can be divided into four general steps:

1. Specimen preparation before data acquisition.
2. Acquiring the X-ray projection images.
3. Computerized reconstruction of 3D of images from the projection images.
4. Analysis of the 3D image stack.

7.4.6a Sample preparation before data acquisition

Specimens from many species can be analysed using micro-CT; however, the examples here are based on the analysis of rabbit mandibles with implanted biomaterials. In several studies, the researchers want to perform histological evaluation on the same samples after micro-CT scanning.

If this is the case, bone samples need to be fixed overnight in 4% buffered formalin after dissection, then washed with PBS and stored in 70% ethanol at 4°C before scanning.

7.4.6b Acquiring the X-ray projection images (scanning)

The first step is to acquire the X-ray images to reconstruct the region of interest. This step is usually referred to as "scanning".

1. Switch on the SkyScan 1172 instrument and the micro-CT computer(s), and open the SkyScan software.
2. Turn on the X-ray source and allow it to run for 10-15 min in order to stabilize the X-ray beam.
3. Set-up the scanning parameters (e.g. voltage, resolution, filtering, etc). The optimal settings depend on the material type, object thickness, scanning medium (air or fluid) and on what needs to be analysed (*see* **Table 7.1, Note 10**).
4. Perform a flat-field correction to correctly calibrate the scanner for the background readings (*see* **Note 11**).
5. Prepare specimen for scanning by removing them from the fixation or storage medium and wrapping them with a Parafilm® to prevent specimen drying (*see* **Note 12**).
6. Mount the specimens in an appropriate holder that is relatively transparent to the X-ray beam (e.g. cylindrical vials from the manufacturer, polystyrene tubes, pipette tips, styrofoams) (*see* **Note 13**).
7. It is preferable that the long axis of the sample to be aligned with the rotation axis of the scanner in order to reduce beam hardening and obtain the best image quality. Once the

sample is loaded in the scanner, a scout scan is performed to set up the appropriate sample position and area of interest. Then, start the scan.

Table 7.1 **Suggested parameters for the scan of specimens using the SkyScan1172 instruments**

Suggested parameters for the scan of rabbit bone specimens using the SkyScan1172 instruments

X-ray voltage	50 kV
X-ray current	200 µA
Filter	0.5 mm aluminum
Camera resolution	Medium
Pixel size	10–15 µm
Tomographic rotation	360°
Rotation step	0.3–0.5
Frame averaging	2–4

7.4.6c Image reconstruction (*see* **Figure 7.4**):

1. After the scan is complete, load the raw image dataset in the NRecon software and select the part of the scan to be reconstructed (avoid including images areas outside of the sample to decrease the dataset size and reconstruction time).
2. Set the reconstruction parameters; beam hardening correction, ring artifact correction, smoothing, and misalignment compensation. The optimal settings need to be empirically evaluated depending on the type of scanner, sample and scanning parameters (*see* **Table 7.2, Note 14**).
3. After selecting the parameters, click on the preview of a single slice to determine whether the settings are correct. Fine-tuning option runs a series of previews by adjusting one parameter or several parameters at the same time in order to select the most optimal setting.

4. Select the data dynamic range from the histogram and select the appropriate image file format (*see* **Note 15**).
5. Create a new folder from the 'raw dataset' folder to save the reconstructed images and run the reconstruction. In case you want to reconstruct more than one sample at the same time, select the "add to batch" option and run the reconstruction after adding the final sample.

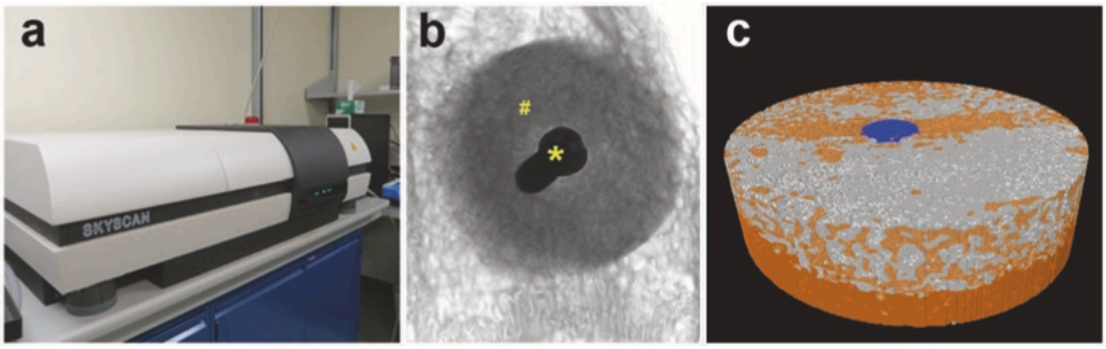

Figure 7.4: An example of Micro-CT analysis. *(a) SkyScan 1172 micro-CT scanner. (b) 2D X-ray projection showing three materials with different X-ray attenuations: titanium screw (*), biomaterial (#) and rabbit bone. (c) 3D reconstructed micro-CT image using CTAn software showing three materials demonstrating a titanium screw (blue), the biomaterial (orange), and the rabbit bone (light grey).*

Table 7.2 ***Image Reconstruction Parameters***

Image reconstruction parameters

Beam hardening correction	20%
Ring artifact correction	10
Smoothing	0
Misalignment compensation	Varied (−0.5 to 1.5)

7.4.6d Analysis of the 3D Image Stack: (*see* Note 16)

1. Upon opening the dataset in CTAn (software provided by SkySkan), select a region of interest (ROI) containing the bone volume that needs to be analyzed around the implanted biomaterials (*see* **Note 17**).
2. Proceed to the binary selection page and choose a threshold range that selects structures to be analyzed, in this case bone, based on gray scale values.
3. Proceed to custom processing and run the thresholding using the selected values. Use despeckling to remove any possible noise "white dots or speckles".
4. Finally, the 3D analysis plug-in can be run to calculate the bone volume within the selected ROI. Several other parameters can be calculated at the same time (e.g. porosity, structure thickness, etc).

7.5 Notes

1. Drugs used will vary according to veterinary instructions.
2. The SkyScan systems are designed to work mainly with standard Microsoft Windows®-based computers.
3. Animals should be sacrificed using procedures approved by animal facility.
4. From this step, the bones are transferred to the tissue culture laboratory for bone marrow harvesting.
5. After 1-2 days, cell pellet forms a round ball. The pellet remains the same size for the entire culture time.
6. Medium are removed carefully to avoid aspirating the pellet.
7. Alternatively, Ca^{2+}- and Mg^{2+}-free HBSS can be used for washing. Cells at passage 3-6 are used for transplantation.
8. Scaffold should be totally immersed in the culture medium.

9. Microcomputed tomography (micro-CT) can be performed either on live animals (in-vivo scanning) or after extracting the specimens from animals (ex-vivo scanning). Several micro-CT systems are available for the study of bone and materials (e.g. Scano, SkyScan, XRadia, etc). Micro-CT measurements vary according to the scanned sample, the scanner used and what needs evaluation. Therefore, this section highlights the points to be considered for micro-CT measurements and focuses on scanning ex-vivo specimens using the SkyScan system.
10. These are the suggested parameters of the scan for our specimen using the SkyScan1172 instruments (**Table 7.1)**.
    - Energy: Higher energy X-ray beam allows better penetration of high-density materials, while low energies yield better contrast when scanning different materials. Therefore, optimal energy is a trade-off between intensity and contrast.
    - Filtering: To minimize the effects of beam hardening, some manufacturers provide a set of filters that can directly absorb the low-energy photons. Using filters narrows the X-ray beam spectrum and makes the images more suitable for quantitative analysis. However, filtering reduces the overall intensity which can be compensated by increasing the exposure time; thus, increasing the overall scanning time.
    - Exposure time: A longer exposure time improves the image quality by reducing noise-to-signal ratio but increases the overall scanning time. However, too high exposure time can fully saturate the micro-CT detector and yield image artifacts.
    - Frame averaging: This option allows imaging each projection several times and using the average for image reconstruction. Similar to increased exposure time, it reduces noise-to-signal ratio, improves the image quality and increases the overall

scanning time. However, the advantage of frame averaging over increasing exposure time is that it avoids saturating the micro-CT detector.

- Resolution: The optimal resolution depends on the specimen size and the features to be analyzed.
- 180^{o} or 360^{o} rotation: 180 degrees scans are used to shorten the overall scanning time, since the projection images from 0-180 degrees are the mirror images of the project images from 180-360 degrees. However, 360 degrees scans are required when scanning complex structures. Moreover, 360 degrees ensures a better quality and more accurate images.

11. Flat-field correction and alignment checks are performed immediately after the installation of the scanner, and repeated every 4 and 8 weeks afterwards, respectively. However, it is recommended to run flat-field correction if the parameters of the scan are changed.
12. Other plastic films can be used that are also relatively transparent to X-rays except the ones containing chloride, since it affects the attenuation of the X-ray beam. Even though micro-CT scanning is a non-destructive method, the heat generated during scanning might dry out the specimen that is why the wrapping step is critical when scanning the specimens in air. On a side note, specimens can be measured both, in air or liquid. In case the specimens need to be measured in liquid (usually saline or 70% ethanol), then avoid creating large air bubbles by adding the liquid slowly using a syringe and then tapping the sample holder to remove any trapped bubbles. Moreover, prevent the liquid from evaporating by closing the sample holder with the provided lid or plastic film.
13. The size of the sample holder depends on the size of the sample and how many samples you want to analyse at the same time using the batch scanning option. In order to obtain an

accurate reconstruction algorithm and prevent motion artifacts, it is critical that there is no relative movement between the specimen and the sample holder during scanning. Therefore, ensure samples fit tightly inside the sample holder by using addition wrapping film, if necessary, without applying too much force to avoid breaking your specimen. Use the most appropriate holder size to avoid using too many wrapping films.

14. We used the following settings in our reconstructions: (*see* **Table 7.2**)
    - Beam hardening is a micro-CT artifact that results due to the fact that the X-ray beam produced by the micro-CT scanner is not composed of single energy X-rays, but rather a spectrum of X-rays. When the X-ray beam hits the sample, the lowest X-ray energies are absorbed first by the outer layers of the samples, while the remaining higher X-rays pass through the rest of the sample. This makes the outer layers of the sample appear as if they have higher X-ray attenuation. The beam hardening correction parameter tries to correct this inherent artifact.
    - Ring artifacts are common artifacts appearing as rings or half-rings in the reconstructed images, attributable to a defect in the scintillator that converts X-ray to visible light, or simply to dust on the detector system. Ring artifact correction tries to replace these artifacts by averaging the neighboring pixels. A higher ring reduction means a more precise reconstruction but increased reconstruction time.
    - Smoothing produces 3D images with less noise; however, it reduces the ability to detect fine details in the sample. Therefore, it is recommended to avoid this option if a precise analysis is required.
    - Misalignment compensation improves the accuracy of reconstruction by compensating for any possible misalignment during acquisition. Misalignment can

differ from sample to sample; however, to compare different samples the other parameters should be the same.

15. This will scale the raw image data set to either 8-bit integer or 16-bit integer image file. Use the same option for all samples in the experiment. (We usually select the JPG file format).
16. Several outcomes can be evaluated from the 3D images (e.g. bone volume, biomaterial volume, bone mineral density, porosity, pore size, etc). It is important to establish a standardized analysis method to be applied to all samples and can be repeated by any user without any bias. The analysis section mentioned here is designed to highlight the steps for measuring bone volume around an implanted biomaterial that has a different X-ray attenuation from the measured bone.
17. To standardize the analysis, use the same ROI shape and size for all samples and with the biomaterial being centered inside the selected ROI. This is why it is important to scan all samples in the same orientation during image acquisition.

7.6 Acknowledgements

We would like to thank the animal resource center at McGill University for the housing and surgery preparation. The authors would like to thank the following funding agency: Natural Sciences and Engineering Research Council of Canada (NSERC), Canadian Institutes of Health Research (CIHR) and Fonds de recherche du Québec-Nature et technologies (FRQNT).

7.7 Author's contribution

This study was designed by Dongdong Fang, Michael Roskies, Mohamed Nur-Abdallah, Faleh Tamimi and Simon Tran. Dongdong Fang and Jack Jordan conducted the isolation and characterization of MSCs; Michael Roskies, Dongdong Fang and Mohamed Bakkar conducted the transplantation of scaffolds. Mohamed Nur-Abdallah contributed to the scaffold analysis and micro-CT scan; All mentioned authors wrote and revised the manuscript. Simon Tran supervised this study and directed final version of all contents. All authors reviewed and approved the manuscript.

8 Conclusion

The is the first investigation of a tissue engineered composite scaffold made with 3D printed porous polyetherketone and stem cells for mandibular reconstruction. The contribution of this body of work is to answer the question of which MSCs demonstrate superior biocompatibility and differentiation on PEK scaffolds (adipose) and to show that a composite scaffold can be implanted without rejection, can integrate into adjacent tissue, can stimulate mineralization and also improve biomechanical resistive strength. Further studies should focus on segmental defects and larger vertebrate models.

9 List of Abbreviations

PEEK – polyetheretherketone

PEKK – polyetherketoneketone

SLS – selective laser sintering

MSC – mesenchymal stem cell

ADSC – adipose-derived MSC

BMSC – bone marrow derived MSC

MicroCT – micro computed tomography or microtomography

SEM – scanning electron microscopy

10 Bibliography & Appendices

1. Reiffel AJ, Kafka C, Hernandez KA, Popa S, Perez JL, Zhou S, et al. High-fidelity tissue engineering of patient-specific auricles for reconstruction of pediatric microtia and other auricular deformities. PloS one. 2013;8(2):e56506.

2. Zopf DA, Hollister SJ, Nelson ME, Ohye RG, Green GE. Bioresorbable airway splint created with a three-dimensional printer. The New England journal of medicine. 2013;368(21):2043-5.

3. Hochman JB, Kraut J, Kazmerik K, Unger BJ. Generation of a 3D printed temporal bone model with internal fidelity and validation of the mechanical construct. Otolaryngology--head and neck surgery : official journal of American Academy of Otolaryngology-Head and Neck Surgery. 2014;150(3):448-54.

4. Cohen A, Laviv A, Berman P, Nashef R, Abu-Tair J. Mandibular reconstruction using stereolithographic 3-dimensional printing modeling technology. Oral surgery, oral medicine, oral pathology, oral radiology, and endodontics. 2009;108(5):661-6.

5. Garcia-Gareta E, Hua J, Blunn GW. Osseointegration of acellular and cellularized osteoconductive scaffolds: is tissue engineering using mesenchymal stem cells necessary for implant fixation? Journal of biomedical materials research Part A. 2015;103(3):1067-76.

6. Jeong WK, Oh SH, Lee JH, Im GI. Repair of osteochondral defects with a construct of mesenchymal stem cells and a polydioxanone/poly(vinyl alcohol) scaffold. Biotechnology and applied biochemistry. 2008;49(Pt 2):155-64.

7. Zamiri B, Shahidi S, Eslaminejad MB, Khoshzaban A, Gholami M, Bahramnejad E, et al. Reconstruction of human mandibular continuity defects with allogenic scaffold and autologous marrow mesenchymal stem cells. The Journal of craniofacial surgery. 2013;24(4):1292-7.

8. Steinberg EL, Rath E, Shlaifer A, Chechik O, Maman E, Salai M. Carbon fiber reinforced PEEK Optima--a composite material biomechanical properties and wear/debris characteristics of CF-PEEK composites for orthopedic trauma implants. Journal of the mechanical behavior of biomedical materials. 2013;17:221-8.

9. Mobbs RJ, Chau AM, Durmush D. Biphasic calcium phosphate contained within a polyetheretherketone cage with and without plating for anterior cervical discectomy and fusion. Orthopaedic surgery. 2012;4(3):156-65.

10. Kim MM, Boahene KD, Byrne PJ. Use of customized polyetheretherketone (PEEK) implants in the reconstruction of complex maxillofacial defects. Archives of facial plastic surgery. 2009;11(1):53-7.

11. Li Z RH, Hauch KD, Xiao D, Zhang M. Chitosan-alginate hybrid scaffolds for bone tissue engineering Biomaterials. 2005;26:3919-28.

12. Rezwan K, Chen QZ, Blaker JJ, Boccaccini AR. Biodegradable and bioactive porous polymer/inorganic composite scaffolds for bone tissue engineering. Biomaterials. 2006;27(18):3413-31.

13. Teven CM, Fisher S, Ameer GA, He TC, Reid RR. Biomimetic approaches to complex craniofacial defects. Annals of maxillofacial surgery. 2015;5(1):4-13.

14. Toth JM, Wang M, Estes BT, Scifert JL, Seim HB, 3rd, Turner AS. Polyetheretherketone as a biomaterial for spinal applications. Biomaterials. 2006;27(3):324-34.

15. Walsh WR, Bertollo N, Christou C, Schaffner D, Mobbs RJ. Plasma sprayed titanium coating to PEEK improves the bone-implant interface. The spine journal : official journal of the North American Spine Society. 2014.

16. Chou YC, Chen DC, Hsieh WA, Chen WF, Yen PS, Harnod T, et al. Efficacy of anterior cervical fusion: comparison of titanium cages, polyetheretherketone (PEEK) cages and autogenous bone grafts. Journal of clinical neuroscience : official journal of the Neurosurgical Society of Australasia. 2008;15(11):1240-5.

17. Wang M, Tang SJ, McGrady LM, Rao RD. Biomechanical comparison of supplemental posterior fixations for two-level anterior lumbar interbody fusion. Proceedings of the Institution of Mechanical Engineers Part H, Journal of engineering in medicine. 2013;227(3):245-50.

18. Williams D. Polyetheretherketone for long-term implantable devices. Medical device technology. 2008;19(1):8, 10-1.

19. Skinner HB. Composite technology for total hip arthroplasty. Clinical orthopaedics and related research. 1988(235):224-36.

20. Kurtz SM. PEEK Biomaterials Handbook. Boston: Amsterdam; 2012.

21. Kurtz SM, Devine JN. PEEK biomaterials in trauma, orthopedic, and spinal implants. Biomaterials. 2007;28(32):4845-69.

22. Walsh WR, Bertollo N, Christou C, Schaffner D, Mobbs RJ. Plasma-sprayed titanium coating to polyetheretherketone improves the bone-implant interface. The spine journal : official journal of the North American Spine Society. 2015;15(5):1041-9.

23. Tan KH, Chua CK, Leong KF, Naing MW, Cheah CM. Fabrication and characterization of three-dimensional poly(ether- ether- ketone)/-hydroxyapatite biocomposite scaffolds using laser sintering. Proceedings of the Institution of Mechanical Engineers Part H, Journal of engineering in medicine. 2005;219(3):183-94.

24. Cancedda R, Giannoni P, Mastrogiacomo M. A tissue engineering approach to bone repair in large animal models and in clinical practice. Biomaterials. 2007;28(29):4240-50.

25. Liang H, Li X, Shimer AL, Balian G, Shen FH. A novel strategy of spine defect repair with a degradable bioactive scaffold preloaded with adipose-derived stromal cells. The spine journal : official journal of the North American Spine Society. 2014;14(3):445-54.

26. Morrison C, Macnair R, MacDonald C, Wykman A, Goldie I, Grant MH. In vitro biocompatibility testing of polymers for orthopaedic implants using cultured fibroblasts and osteoblasts. Biomaterials. 1995;16(13):987-92.

27. Neuss S, Apel C, Buttler P, Denecke B, Dhanasingh A, Ding X, et al. Assessment of stem cell/biomaterial combinations for stem cell-based tissue engineering. Biomaterials. 2008;29(3):302-13.

28. Garcia-Gareta E, Hua J, Blunn GW. Osseointegration of acellular and cellularized osteoconductive scaffolds: Is tissue engineering using mesenchymal stem cells necessary for implant fixation? Journal of biomedical materials research Part A. 2014.

29. Koyanagi H, Ae K, Maehara H, Yuasa M, Masaoka T, Yamada T, et al. Massive bone reconstruction with heat-treated bone graft loaded autologous bone marrow-derived stromal cells and beta-tricalcium phosphate composites in canine models. Journal of orthopaedic research : official publication of the Orthopaedic Research Society. 2013;31(8):1308-16.

30. Lu W, Ji K, Kirkham J, Yan Y, Boccaccini AR, Kellett M, et al. Bone tissue engineering by using a combination of polymer/Bioglass composites with human adipose-derived stem cells. Cell and tissue research. 2014;356(1):97-107.

31. Victrex PEEK 450G. Victrex PEEK polymer properties guide. Lacashire, UK2014.

32. Bunnell BA, Flaat M, Gagliardi C, Patel B, Ripoll C. Adipose-derived stem cells: isolation, expansion and differentiation. Methods. 2008;45(2):115-20.

33. Maniatopoulos C, Sodek J, Melcher AH. Bone formation in vitro by stromal cells obtained from bone marrow of young adult rats. Cell and tissue research. 1988;254(2):317-30.

34. Bruedigam C, Driel M, Koedam M, Peppel J, van der Eerden BC, Eijken M, et al. Basic techniques in human mesenchymal stem cell cultures: differentiation into osteogenic and adipogenic lineages, genetic perturbations, and phenotypic analyses. Current protocols in stem cell biology. 2011;Chapter 1:Unit1H 3.

35. Eijken M, Swagemakers S, Koedam M, Steenbergen C, Derkx P, Uitterlinden AG, et al. The activin A-follistatin system: potent regulator of human extracellular matrix mineralization. FASEB journal : official publication of the Federation of American Societies for Experimental Biology. 2007;21(11):2949-60.

36. Hasegawa T, Miwa M, Sakai Y, Niikura T, Lee SY, Oe K, et al. Efficient cell-seeding into scaffolds improves bone formation. Journal of dental research. 2010;89(8):854-9.

37. Landy BC, Vangordon SB, McFetridge PS, Sikavitsas VI, Jarman-Smith M. Mechanical and in vitro investigation of a porous PEEK foam for medical device implants. Journal of applied biomaterials & functional materials. 2013;11(1):e35-44.

38. Zhang H. Fire-Safe Polymers and Polymer Composites. 2004.

39. Abu Bakar MS, Cheng MH, Tang SM, Yu SC, Liao K, Tan CT, et al. Tensile properties, tension-tension fatigue and biological response of polyetheretherketone-hydroxyapatite composites for load-bearing orthopedic implants. Biomaterials. 2003;24(13):2245-50.

40. Waser-Althaus J, Salamon A, Waser M, Padeste C, Kreutzer M, Pieles U, et al. Differentiation of human mesenchymal stem cells on plasma-treated polyetheretherketone. Journal of materials science Materials in medicine. 2014;25(2):515-25.

41. Tuan RS, Boland G, Tuli R. Adult mesenchymal stem cells and cell-based tissue engineering. Arthritis research & therapy. 2003;5(1):32-45.

42. Zielins ER, Tevlin R, Hu MS, Chung MT, McArdle A, Paik KJ, et al. Isolation and enrichment of human adipose-derived stromal cells for enhanced osteogenesis. Journal of visualized experiments : JoVE. 2015(95):52181.

43. Suh JD, Sercarz JA, Abemayor E, Calcaterra TC, Rawnsley JD, Alam D, et al. Analysis of outcome and complications in 400 cases of microvascular head and neck reconstruction. Archives of otolaryngology--head & neck surgery. 2004;130(8):962-6.

44. Disa JJ, Hu QY, Hidalgo DA. Retrospective review of 400 consecutive free flap reconstructions for oncologic surgical defects. Annals of surgical oncology. 1997;4(8):663-9.

45. Buck D, 2nd, Rawlani V, Wayne J, Dumanian GA, Mustoe TA, Fine NA, et al. Cosmetic outcomes following head and neck melanoma reconstruction: The patient's perspective. The Canadian journal of plastic surgery = Journal canadien de chirurgie plastique. 2012;20(1):e10-5.

46. Johansson P, Jimbo R, Kjellin P, Currie F, Chrcanovic BR, Wennerberg A. Biomechanical evaluation and surface characterization of a nano-modified surface on PEEK implants: a study in the rabbit tibia. International journal of nanomedicine. 2014;9:3903-11.

47. Vaidya R, Sethi A, Bartol S, Jacobson M, Coe C, Craig JG. Complications in the use of rhBMP-2 in PEEK cages for interbody spinal fusions. Journal of spinal disorders & techniques. 2008;21(8):557-62.

48. Roskies M, Jordan JO, Fang D, Abdallah MN, Hier MP, Mlynarek A, et al. Improving PEEK bioactivity for craniofacial reconstruction using a 3D printed scaffold embedded with mesenchymal stem cells. Journal of biomaterials applications. 2016;31(1):132-9.

49. Matsiko A, Gleeson JP, O'Brien FJ. Scaffold mean pore size influences mesenchymal stem cell chondrogenic differentiation and matrix deposition. Tissue engineering Part A. 2015;21(3-4):486-97.

50. Tiainen H, Lyngstadaas SP, Ellingsen JE, Haugen HJ. Ultra-porous titanium oxide scaffold with high compressive strength. Journal of Materials Science: Materials in Medicine. 2010;21(10):2783-92.

51. Cheng G, Li Z, Wan Q, Lv K, Li D, Xing X, et al. A novel animal model treated with tooth extraction to repair the full-thickness defects in the mandible of rabbits. The Journal of surgical research. 2015;194(2):706-16.

52. Bobyn JD, Stackpool GJ, Hacking SA, Tanzer M, Krygier JJ. Characteristics of bone ingrowth and interface mechanics of a new porous tantalum biomaterial. The Journal of bone and joint surgery British volume. 1999;81(5):907-14.

53. Barralet JE, Gaunt T, Wright AJ, Gibson IR, Knowles JC. Effect of porosity reduction by compaction on compressive strength and microstructure of calcium phosphate cement. Journal of biomedical materials research. 2002;63(1):1-9.

54. Shan X F, Chen H M, Liang J, Huang J W, Cai Z G (2015) Surgical Reconstruction of Maxillary and Mandibular Defects Using a Printed Titanium Mesh. *J Oral Maxillofac Surg* 73 (7):1437.e1431-1439.

55. Liu C, Tan X, Luo J, Liu H, Hu M, Yue W (2014) Reconstruction of beagle hemi-mandibular defects with allogenic mandibular scaffolds and autologous mesenchymal stem cells. *PLoS One* 9 (8):e105733.

56. Liu S P, Cai Z G, Zhang J, Zhang J G, Zhang Y (2015) Stability and complications of miniplates for mandibular reconstruction with a fibular graft: outcomes for 544 patients. *Br J Oral Maxillofac Surg*.

57. Dimitriou R, Mataliotakis G I, Angoules A G, Kanakaris N K, Giannoudis P V (2011) Complications following autologous bone graft harvesting from the iliac crest and using the RIA: a systematic review. *Injury* 42 Suppl 2:S3-15.

58. Alfotawei R, Naudi K B, Lappin D, Barbenel J, Di Silvio L, Hunter K, McMahon J, Ayoub A (2014) The use of TriCalcium Phosphate (TCP) and stem cells for the regeneration of osteoperiosteal critical-size mandibular bony defects, an in vitro and preclinical study. *J Craniomaxillofac Surg* 42 (6):863-869.

59. Yuan J, Cui L, Zhang W J, Liu W, Cao Y (2007) Repair of canine mandibular bone defects with bone marrow stromal cells and porous beta-tricalcium phosphate. *Biomaterials* 28 (6):1005-1013.

60. Arinzeh T L, Peter S J, Archambault M P, van den Bos C, Gordon S, Kraus K, Smith A, Kadiyala S (2003) Allogeneic mesenchymal stem cells regenerate bone in a critical-sized canine segmental defect. *J Bone Joint Surg Am* 85-a (10):1927-1935.

61. Jones E, McGonagle D (2008) Human bone marrow mesenchymal stem cells in vivo. *Rheumatology (Oxford)* 47 (2):126-131.

62. Pittenger M F, Mackay A M, Beck S C, Jaiswal R K, Douglas R, Mosca J D, Moorman M A, Simonetti D W, Craig S, Marshak D R (1999) Multilineage potential of adult human mesenchymal stem cells. *Science* 284 (5411):143-147.

63. Zuk P A, Zhu M, Mizuno H, Huang J, Futrell J W, Katz A J, Benhaim P, Lorenz H P, Hedrick M H (2001) Multilineage cells from human adipose tissue: implications for cell-based therapies. *Tissue Eng* 7 (2):211-228.

64. Zuk P A, Zhu M, Ashjian P, De Ugarte D A, Huang J I, Mizuno H, Alfonso Z C, Fraser J K, Benhaim P, Hedrick M H (2002) Human adipose tissue is a source of multipotent stem cells. *Mol Biol Cell* 13 (12):4279-4295.

65. Guilak F, Lott K E, Awad H A, Cao Q, Hicok K C, Fermor B, Gimble J M (2006) Clonal analysis of the differentiation potential of human adipose-derived adult stem cells. *J Cell Physiol* 206 (1):229-237.

66. Wen C, Yan H, Fu S, Qian Y, Wang D, Wang C (2015) Allogeneic adipose-derived stem cells regenerate bone in a critical-sized ulna segmental defect. *Exp Biol Med (Maywood)*.

67. Semyari H, Rajipour M, Sabetkish S, Sabetkish N, Abbas F M, Kajbafzadeh A M (2015) Evaluating the bone regeneration in calvarial defect using osteoblasts differentiated from adipose-derived mesenchymal stem cells on three different scaffolds: an animal study. *Cell Tissue Bank*.

68. Viateau V, Guillemin G, Bousson V, Oudina K, Hannouche D, Sedel L, Logeart-Avramoglou D, Petite H (2007) Long-bone critical-size defects treated with tissue-engineered grafts: a study on sheep. *J Orthop Res* 25 (6):741-749.

69. Bruder S P, Kraus K H, Goldberg V M, Kadiyala S (1998) The effect of implants loaded with autologous mesenchymal stem cells on the healing of canine segmental bone defects. *J Bone Joint Surg Am* 80 (7):985-996.

70. Zhou Y F, Sae-Lim V, Chou A M, Hutmacher D W, Lim T M (2006) Does seeding density affect in vitro mineral nodules formation in novel composite scaffolds? *J Biomed Mater Res A* 78 (1):183-193.

71. Lode A, Bernhardt A, Gelinsky M (2008) Cultivation of human bone marrow stromal cells on three-dimensional scaffolds of mineralized collagen: influence of seeding density on colonization, proliferation and osteogenic differentiation. *J Tissue Eng Regen Med* 2 (7):400-407.